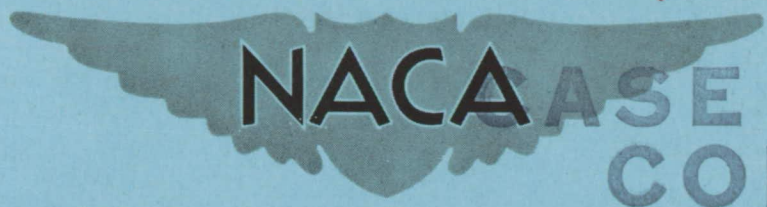


CONFIDENTIAL

1523

1523

NACA RM L52L11b



NACA CASE FILE COPY

RESEARCH MEMORANDUM

LOW-SPEED LONGITUDINAL CHARACTERISTICS
OF AN UNSWEPT HEXAGONAL WING WITH AND WITHOUT A FUSELAGE
AND A HORIZONTAL TAIL LOCATED AT VARIOUS POSITIONS
AT REYNOLDS NUMBERS FROM 2.8×10^6 TO 7.6×10^6

By Gerald V. Foster, Ernst F. Mollenberg,
and Robert L. Woods

Langley Aeronautical Laboratory
Langley Field, Va.

CLASSIFICATION CHANGED TO UNCLASSIFIED

AUTHORITY: NACA RESEARCH ABSTRACT NO. 94

DATE: JANUARY 11, 1956
CLASSIFIED DOCUMENT

WHL

This material contains information affecting the National Defense of the United States within the meaning of the espionage laws, Title 18, U.S.C., Secs. 793 and 794, the transmission or revelation of which in any manner to an unauthorized person is prohibited by law.

NATIONAL ADVISORY COMMITTEE FOR AERONAUTICS

WASHINGTON
February 26, 1953

CONFIDENTIAL

NATIONAL ADVISORY COMMITTEE FOR AERONAUTICS

RESEARCH MEMORANDUM

LOW-SPEED LONGITUDINAL CHARACTERISTICS
OF AN UNSWEPT HEXAGONAL WING WITH AND WITHOUT A FUSELAGE
AND A HORIZONTAL TAIL LOCATED AT VARIOUS POSITIONS
AT REYNOLDS NUMBERS FROM 2.8×10^6 TO 7.6×10^6

By Gerald V. Foster, Ernst F. Mollenberg,
and Robert L. Woods

SUMMARY

An investigation has been conducted to determine the low-speed static longitudinal characteristics of an unswept wing having hexagonal airfoil sections and an aspect ratio of 2.5. The wing with and without a fuselage was tested with plain flaps (with several degrees of trailing-edge bluntness) and nose flaps deflected individually and in combination. The effect of a horizontal tail on the wing-fuselage configuration was investigated at various vertical and horizontal positions. The tests were conducted at Reynolds numbers ranging from 2.8×10^6 to 7.6×10^6 and Mach numbers ranging from 0.05 to 0.15.

A brief analysis of these data indicates that the wing exhibited leading-edge separation at a low angle of attack which produced a rapid increase in drag and a stabilizing change in the pitching-moment characteristics. The drooped-nose flaps delayed the leading-edge separation and the associated changes in the drag and pitching-moment characteristics. The stabilizing effect of the horizontal tail varied with vertical position in a manner similar to that shown by previous investigations of swept wings; however, the change of static margin through the lift range obtained with the horizontal tail located 0.40 semispan above the wing-chord plane appeared, in most cases, more favorable than that obtained with the horizontal tail located 0.177 semispan below the wing-chord plane.

INTRODUCTION

Theoretical and experimental investigations indicate that thin, unswept, low-aspect-ratio wings can in many instances be advantageously

incorporated in the design of airplanes intended for flight at high supersonic speeds. In order to determine the low-speed aerodynamic characteristics of such a wing, tests of a wing having an aspect ratio of 2.5 and 6-percent-thick, hexagonal airfoil sections have been conducted in the Langley 19-foot pressure tunnel. Reference 1 presents the lateral-control characteristics of the wing equipped with spoilers and with ailerons. The results of the investigation pertaining to the longitudinal characteristics of the wing are presented herein.

Inasmuch as a relatively low maximum lift coefficient was expected for the wing because of flow separation promoted by the sharp leading edge, tests were made to determine the separate and combined effects of drooped-nose flaps and plain flaps on the longitudinal characteristics of the wing with and without a fuselage. The effects of a horizontal tail on the longitudinal stability characteristics of the wing-fuselage configuration were investigated with the tail located at various vertical and horizontal positions. In order to expedite the issuance of this information, only a brief analysis has been made of these data.

The data presented herein were obtained at Reynolds numbers ranging from 2.8×10^6 to 7.6×10^6 and Mach numbers ranging from 0.05 to 0.15.

SYMBOLS

C_L	lift coefficient, Lift/qS
ΔC_L	increment of lift coefficient
$C_{L_{max}}$	maximum lift coefficient
C_D	drag coefficient, Drag/qS
C_m	pitching-moment coefficient, moment about the quarter chord of mean aerodynamic chord, Pitching moment/q \bar{c} S
S	area (wing area unless otherwise noted), sq ft
\bar{c}	mean aerodynamic chord measured parallel to the plane of symmetry, $\frac{2}{S} \int_0^{b/2} c^2 dy$, ft
b	wing span, ft
c	local wing chord, ft

y	spanwise ordinate, ft
q	free-stream dynamic pressure, $\rho V^2/2$; lb/sq ft
ρ	mass density of air, slugs/cu ft
α	angle of attack of wing chord, deg
V	free-stream velocity, ft/sec
R	Reynolds number (based on \bar{c})
τ	horizontal-tail effectiveness parameter
$(C_{L\alpha})_t$	lift-curve slope of isolated horizontal tail
$(q_t/q)_e$	ratio of effective dynamic pressure to free-stream dynamic pressure
ϵ_e	effective downwash angle, deg
$C_{m_{i_t}}$	rate of change of pitching-moment coefficient with horizontal-tail incidence angle
$(C_{m_{i_t}})'_o$	value of dC_m/di_t at zero lift for a high tail position with flaps off (assumed interference free condition)
$dC_{m_t}/d\alpha$	rate of change of pitching-moment coefficient due to the tail with angle of attack
η	tail efficiency factor, $(C_{m_{i_t}})'_o / (C_{m_{i_t}})'_o$
i_t	angle of incidence of horizontal tail measured with respect to wing-chord plane, positive when trailing edge moves down, deg
l	horizontal-tail length, distance in wing-chord plane from quarter-chord point of wing mean aerodynamic chord to quarter-chord point of the horizontal tail mean aerodynamic chord, ft
δ_f	angle of deflection of plain flaps, deg
δ_n	angle of deflection of drooped-nose flaps, deg
$d\epsilon_e/d\alpha$	rate of change of effective downwash angle with angle of attack

- z vertical position of horizontal tail from wing-root chord plane (positive above)
- t maximum thickness of wing airfoil section
- f_r fineness ratio of fuselage

Subscripts and abbreviations:

- t horizontal tail
- o value at zero lift
- e effective

MODEL AND TESTS

Model

The details of the wing, fuselage, and horizontal tail are shown in figure 1. The wing had an aspect ratio of 2.5, a taper ratio of 0.625, and neither twist nor dihedral. The wing had sharp leading and trailing edges formed by wedges which extended 30 percent of the chord. The upper and lower surfaces of the middle 40 percent chord of the wing were parallel and 6 percent of the chord apart. The wing was provided with interchangeable tips having wedge and elliptical cross sections (fig. 1). In a few instances the trailing-edge thickness of the wing was increased to 0.25, 0.50, and 1.00 of the maximum local thickness.

The wing was equipped with drooped-nose flaps at the leading edge and plain flaps at the trailing edge. The drooped-nose flaps of 15 percent chord extended spanwise from 20 percent wing semispan to 95 percent wing semispan and could be deflected 10° , 20° , or 30° . The plain flaps of 25 percent chord extended from 20 percent (wing-fuselage juncture) to 55 percent wing semispan and from 20 percent to 95 percent wing semispan.

A fuselage of circular cross section used in combination with the wing was attached in a midwing arrangement at zero incidence. The fuselage was provided with two different afterbodies which were used alternately to provide tail lengths of either 2 or 3 mean aerodynamic chords. The fineness ratio of the fuselage was either 8 or 10, depending on the fuselage afterbody used.

The horizontal tail had NACA 0012 airfoil sections parallel to the plane of symmetry, an aspect ratio of 3.12, and a taper ratio of 0.625. The ratio of tail area to wing area was 0.200. The tail was

attached to the fuselage by means of a strut and could be located vertically at either 40.0 or 17.7 percent wing semispan above or 17.7 percent wing semispan below the wing chord plane extended. The incidence of the tail, measured with respect to the wing chord plane, could be varied through an angle range of 2° to -6° .

Tests

Tests were conducted in the Langley 19-foot pressure tunnel to determine the longitudinal aerodynamic characteristics of the wing and the effects thereupon of various flaps, a fuselage, and a horizontal tail located at various vertical and horizontal positions. The longitudinal characteristics were determined by measuring the lift, drag, and pitching moment through an angle-of-attack range of -4° to stall. Tests to determine the air-flow characteristics at the wing surface also were made by observation of wool tufts that were attached to the upper surface of the wing. The various configurations tested are listed in tables I and II.

The maximum Reynolds number of the tests of the model with 0.35b plain flaps either in a neutral or deflected position was 7.6×10^6 . For tests of the model with 0.75b plain flaps deflected, the Reynolds number was 5.4×10^6 . The Mach number of the tests ranged from 0.05 to 0.15.

A two-support system was used in testing all model configurations except tail-on configurations for which a three-support system was used (fig. 2).

As an aid in the analysis of these data, the tail was tested independently at Reynolds numbers of 2.3×10^6 and 3.0×10^6 which corresponds to wing Reynolds numbers of 5.7×10^6 and 7.5×10^6 .

RESULTS

Reduction of Data

The results of tests have been reduced to nondimensional-coefficient form and, with the exception of the results of isolated tail tests, have been corrected for support-strut tare and interference. The angles of attack have been corrected for air-stream misalignment and jet-boundary effects. Jet-boundary corrections also were applied to the drag characteristics of all configurations and pitching-moment characteristics of the tail-on configurations. The jet-boundary corrections were determined by the method of reference 2.

The values of effective downwash angle were determined from data obtained at three tail incidence angles. The pitching-moment coefficient due to the tail C_{m_t} was plotted against the tail incidence angle i_t for various values of the wing angle of attack α . The intersection of the faired points with the C_{m_t} zero axis indicated the tail incidence angle for which the angle of attack of the tail was zero. The effective downwash angle ϵ_e was then obtained from the relation

$$\epsilon_e = \alpha + i_t - \alpha_t \quad (1)$$

The values of effective dynamic pressure ratio at the tail $(q_t/q)_e$ were determined by computing the ratio of the values $C_{m_{i_t}}$ obtained through the angle-of-attack ranges of the various configurations to the value of $C_{m_{i_t}}$ for the comparable tail height of the flap-neutral configuration at zero lift.

The tail efficiency factor η represents the effective change in the lift-curve slope of the tail due to the effect of the fuselage interference. The values of η are based on the assumption that the efficiency of the tail located at $z = 0.40b/2$ was 100 percent inasmuch as the distance from the fuselage was large and the interference effect of the tail post would be small. The values of η were obtained from the relation

$$\eta = \frac{(C_{m_{i_t}})_o}{(C_{m_{i_t}})_o'} \quad (2)$$

The following table presents values of $(C_{m_{i_t}})_o$ and η for the flap-neutral configuration:

Tail Height	Tail length, $2\bar{c}$		Tail length, $3\bar{c}$	
	$(C_{m_{i_t}})_o$	η	$(C_{m_{i_t}})_o$	η
0.400b/2	-0.0202	1.00	-0.0302	1.00
.177b/2	-.0189	.94	-.0287	.95
-.177b/2	-.0190	.94	-.0280	.93

The values of η presented are also representative of the values obtained for configurations with flaps deflected.

The contribution of the tail to the stability can be conveniently expressed by a tail effectiveness parameter τ derived in reference 3, which is defined as follows:

$$\tau = - \left[\left(1 - \frac{d\epsilon}{d\alpha} \right) \frac{q_t}{q} + \alpha_t \frac{d\left(\frac{q_t}{q}\right)}{d\alpha} \right] \eta \quad (3)$$

or

$$\tau = \frac{\frac{dC_{m_t}}{d\alpha}}{\frac{S_t}{S} \frac{l}{\bar{c}} (C_{L_\alpha})_t} \quad (4)$$

where

$$(C_{L_\alpha})_t = 0.050 \text{ per degree}$$

Figure 3 shows the variation of lift coefficient with angle of attack of the isolated tail. A negative value of τ signifies that the tail is contributing to the stability.

The values of τ presented herein were obtained with a fixed tail incidence, and, consequently, large out-of-trim conditions occurred at high angles of attack. Examination of equation (3) shows that, for finite values of α_t , τ is affected by the variation of q_t/q with α . For the condition where the tail is free of the wake and the values of $\frac{d\left(\frac{q_t}{q}\right)}{d\alpha}$ are negligible, the values of τ are independent of tail load and hence are applicable to any center-of-gravity location or tail incidence angle. Through the angle-of-attack range for which the tail passes through the wake finite values of $\frac{d\left(\frac{q_t}{q}\right)}{d\alpha}$ are obtained; hence, the values of τ for that angle-of-attack range are more nearly representative of a center-of-gravity location for which the measured tail load would provide trim at the wake center.

Presentation of Data

Data showing the effects of Reynolds numbers ranging from 2.8×10^6 to 7.6×10^6 , wing trailing-edge thickness, and cross-sectional shape of the wing tip on the longitudinal characteristics of the wing are presented in figures 4 to 6. The effects of plain flaps and drooped-nose flaps deflected individually and in combination on the wing are indicated by the data presented in figures 7 to 13. Figure 14 shows the flow patterns of the wing with and without flaps deflected. The effects of flaps on the longitudinal characteristics of the wing in combination with a fuselage are indicated by the data presented in figures 15 to 18. The effects of the various arrangements of flaps on the lift characteristics of the wing with and without a fuselage are summarized in figure 19. The effect on the longitudinal stability characteristics of the wing-fuselage configuration of a horizontal tail located at various vertical and horizontal positions is shown by the data presented in figures 20 to 24.

An index of the various configurations tested and a summary of the longitudinal stability characteristics has been presented in tables I, II, and III.

BRIEF ANALYSIS OF DATA

Wing Configurations

The wing exhibited leading-edge separation characteristic of sharp-edge airfoil sections at a low angle of attack (fig. 14) and, consequently, an increase in stability (fig. 4) associated with a rearward shift of the center of pressure was obtained. The lift-drag ratio of the wing decreased rapidly with the onset of separation from a maximum value of approximately 12 to approximately 3 at maximum lift (fig. 4). It is of interest to note that, contrary to the results shown in reference 4, a small destabilizing change in the pitching-moment characteristics and an increase in the slope of lift curve occurred in the low angle-of-attack range of the wing with increase in Reynolds number through the range investigated (fig. 4). The maximum lift coefficient of the wing was increased from 0.71 to 1.07 with the 0.35b plain flaps ($\delta_f = 50^\circ$) and to 1.34 with the 0.75b plain flaps ($\delta_f = 50^\circ$), (fig. 19(a)). With the drooped-nose flaps deflected, the initial leading-edge separation occurred at approximately the same angle of attack as the plain wing but was confined to the inboard 20-percent wing semispan where the leading edge was not drooped rather than along the entire leading edge. Separation then spread rearward and outboard as the angle of attack was increased; however, the flow in the region of the tips remained unseparated through the stall with the drooped-nose flaps deflected 30° .

(fig. 14). The delay of separation over the outboard sections of the wings caused by drooped-nose flaps deflected at least 20° minimized the large stabilizing change in the pitching-moment characteristics through a lift-coefficient range to just prior to $C_{L_{max}}$ (fig. 10). The summary of lift characteristics (fig. 19) indicate that the sum of increments of maximum lift contributed by plain flaps and drooped-nose flaps considerably exceeded the increment of maximum lift obtained for the wing equipped with plain flaps and drooped-nose flaps in combination.

Wing-Fuselage Configuration

The results of figure 19 indicate that the addition of the fuselage increased the maximum lift coefficient of the wing equipped with drooped-nose flaps as much as 0.2 ($\delta_n = 30^\circ$) but had a negligible effect on the maximum lift coefficient of the wing equipped with plain flaps. In general, the results for the wing-fuselage configuration either with or without flaps indicate a fairly large forward shift of the aerodynamic center as compared with the wing alone.

Wing-Fuselage Configuration in Combination

With a Horizontal Tail

In general, all tail-on configurations investigated exhibited static longitudinal stability throughout the lift range for the center of gravity at $0.25\bar{c}$. The effect of vertical position of the horizontal tail on the tail effectiveness is similar to that reported for swept-wing airplane configurations (refs. 3 and 5). The values of τ (figs. 20 to 23) indicate that the horizontal tail was more effective through the moderate and high angle-of-attack range when located $0.177b/2$ below the wing-chord plane than when located at either $0.177b/2$ or $0.40b/2$ above the wing-chord plane. This is attributed to a smaller variation of downwash angle with angle of attack just below the wake center line than just above the wake center line. The pitching-moment characteristics (table II) tend to indicate that, although the change of static margin through the lift range was large for all tail-on configurations, the change of static margin through the lift range obtained with the horizontal tail located 0.40 semispan above the wing chord

plane appeared, in most cases, more favorable than that obtained with the horizontal tail located 0.177 semispan below the wing chord plane.

Langley Aeronautical Laboratory,
National Advisory Committee for Aeronautics,
Langley Field, Va.

REFERENCES

1. Fitzpatrick, James E., and Woods, Robert L.: Low-Speed Lateral-Control Characteristics of an Unswept Wing With Hexagonal Airfoil Sections and Aspect Ratio 2.5 Equipped With Spoilers and With Sharp- and Thickened-Trailing-Edge Flap-Type Ailerons at a Reynolds Number of 7.6×10^6 . NACA RM L52B15, 1952.
2. Silverstein, Abe, and White, James A.: Wind-Tunnel Interference With Particular Reference to Off-Center Positions of the Wing and to the Downwash at the Tail. NACA Rep. 547, 1936.
3. Foster, Gerald V., and Griner, Roland F.: Low-Speed Longitudinal and Wake Air-Flow Characteristics at a Reynolds Number of 5.5×10^6 of a Circular-Arc 52° Sweptback Wing With a Fuselage and a Horizontal Tail at Various Vertical Positions. NACA RM L51C30, 1951.
4. Johnson, Ben H., Jr.: Investigation of a Thin Wing of Aspect Ratio 4 in the Ames 12-Foot Pressure Wind Tunnel. I - Characteristics of a Plain Wing. NACA RM A8D07, 1948.
5. Griner, Roland F., and Foster, Gerald V.: Low-Speed Longitudinal and Wake Air-Flow Characteristics at a Reynolds Number of 6.0×10^6 of a 52° Sweptback Wing Equipped With Various Spans of Leading-Edge and Trailing-Edge Flaps, a Fuselage, and a Horizontal Tail at Various Vertical Positions. NACA RM L50K29, 1951.

TABLE I.- INDEX OF TEST CONFIGURATIONS OF WING

Wing trailing-edge thickness	Tip cross section	Plain flaps	Drooped-nose flaps	Presented	Figure
0.0t	Wedge	Off	Off	C_L, C_D, C_m	4
0.0t .015t .030t .060t	Wedge	Off	Off	C_L, C_D, C_m	5
0.0t	Wedge and elliptical	Off	Off	C_L, C_D, C_m	6
0.0t	Wedge	0.35b $\delta_f = 0^\circ, 30^\circ, 40^\circ, 50^\circ$	Off	C_L, C_D, C_m	7
0.0t	Wedge	0.75b $\delta_f = 0^\circ, 30^\circ, 40^\circ, 50^\circ$	Off	C_L, C_D, C_m	8
0.0t .015t .030t .060t	Wedge	0.75b $\delta_f = 50^\circ$	Off	C_L, C_D, C_m	9
0.0t	Wedge	Off	$\delta_n = 0^\circ, 10^\circ, 20^\circ, 30^\circ$	C_L, C_D, C_m	10
0.0t	Wedge	Off 0.35b - 50° 0.75b - 50°	$\delta_n = 10^\circ$	C_L, C_D, C_m	11
0.0t	Wedge	Off 0.35b - 50° 0.75b - 50°	$\delta_n = 20^\circ$	C_L, C_D, C_m	12
0.0t	Wedge	Off 0.35b - 50° 0.75b - 50°	$\delta_n = 30^\circ$	C_L, C_D, C_m	13



TABLE II.- INDEX OF TEST CONFIGURATIONS OF WING IN COMBINATION WITH FUSELAGE

Wing	Plain flaps	Drooped-nose flaps	Tail		Presented	Figure
			Length	Height		
Basic wing ^a	Off 0.35b - 50° 0.75b - 50°	Off	--	Off	C_L, C_D, C_m	15
	Off 0.35b - 50° 0.75b - 50°	$\delta_n = 10^\circ$	--	Off	C_L, C_D, C_m	16
	Off 0.35b - 50° 0.75b - 50°	$\delta_n = 20^\circ$	--	Off	C_L, C_D, C_m	17
	Off 0.35b - 50° 0.75b - 50°	$\delta_n = 30^\circ$	--	Off	C_L, C_D, C_m	18
	Off	Off	2c̄	Off -0.177b/2 .177 .400	$C_L, C_m, \epsilon_e,$ $(q_t/q)_e$ and τ	20(a)
				Off -0.177b/2 .177 .400		
	Off	$\delta_n = 30^\circ$	2c̄	Off -0.177b/2 .177 .400	$C_L, C_m, \epsilon_e,$ $(q_t/q)_e$ and τ	21
	0.35b $\delta_f = 50^\circ$	$\delta_n = 30^\circ$	2c̄	Off -0.177b/2 .177 .400	$C_L, C_m, \epsilon_e,$ $(q_t/q)_e$ and τ	22(a)
				Off -0.177b/2 .177 .400		
	0.75b $\delta_f = 50^\circ$	$\delta_n = 30^\circ$	2c̄	Off -0.177b/2 .177 .400	$C_L, C_m, \epsilon_e,$ $(q_t/q)_e$ and τ	23(a)
				Off -0.177b/2 .177 .400		

^aDenotes wing having 0.0t thickness at trailing edge and wedge-shape cross sections at the tips.

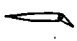
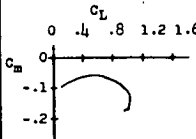
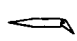
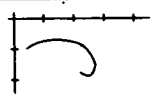
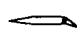
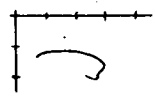
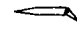
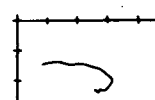
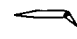
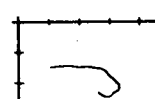
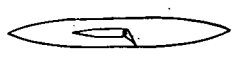
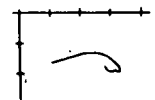

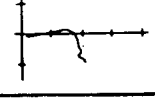
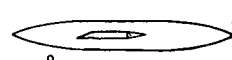
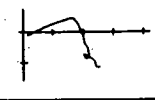

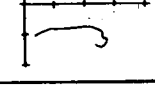
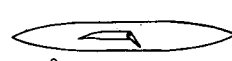
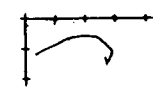

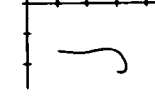


TABLE III.- SUMMARY OF LONGITUDINAL STABILITY CHARACTERISTICS OF AN UNSWEPT WING
HAVING THIN HEXAGONAL AIRFOIL SECTIONS AND AN ASPECT RATIO OF 2.5

Span of L.E. Device (b/2)	Span of T.E. Device (b/2)	Configuration	$C_{L_{max}}$	$\alpha_{C_{L_{max}}}$	L/D at $0.85 C_{L_{max}}$	C_m Characteristics	Figure
None	None		.725	14.7°	5.32		4
							15 and 20(a)
							20(a)
							20(a)
							20(a)
							20(b)
							20(b)
							20(b)
							20(b)
		.35 T.E. Flap			.955	12.9°	6.98



TABLE III.- SUMMARY OF LONGITUDINAL STABILITY CHARACTERISTICS OF AN UNSWEPT WING HAVING THIN HEXAGONAL AIRFOIL SECTIONS AND AN ASPECT RATIO OF 2.5 - Continued

Span of L.E. Device (b/2)	Span of T.E. Device (b/2)	Configuration	$C_{l_{max}}$	$\alpha_{C_{l_{max}}}$	L/D at $0.85 C_{l_{max}}$	C_m Characteristics	Figure
None	.35 T.E. Flaps	 $\delta_f = 40^\circ$	1.025	12.9°	4.85		7
		 $\delta_f = 50^\circ$	1.070	13.0°	4.29		7
	.75 T.E. Flaps	 $\delta_f = 30^\circ$	1.16	12.0°	4.58		8
		 $\delta_f = 40^\circ$	1.26	12.1°	3.96		8
		 $\delta_f = 50^\circ$	1.34	12.2°	3.59		8
		 $\delta_f = 50^\circ$					15
.775 L.E. Droop	None	 $\delta_n = 10^\circ$	*0.84	21.8	5.25		10
		 $\delta_n = 10^\circ$					16 and 21
	.35 T.E. Flaps	 $\delta_n = 10^\circ$ $\delta_f = 50^\circ$	1.09	14.2	4.41		11
		 $\delta_n = 10^\circ$ $\delta_f = 50^\circ$					16
	.75 T.E. Flaps	 $\delta_n = 10^\circ$ $\delta_f = 50^\circ$	1.38	14.2	3.44		11

* $C_{l_{max}}$ not reached.



TABLE III.- SUMMARY OF LONGITUDINAL STABILITY CHARACTERISTICS OF AN UNSWEPT WING HAVING THIN HEXAGONAL AIRFOIL SECTIONS AND AN ASPECT RATIO OF 2.5 - Continued

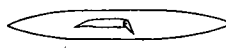
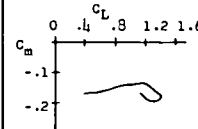
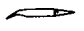
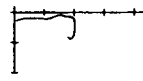
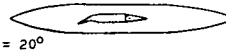
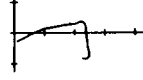
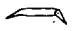
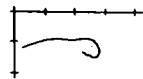
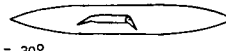
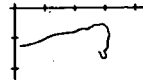
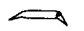
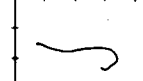
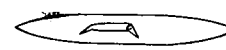
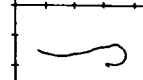
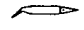
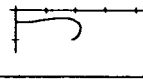
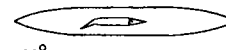
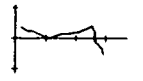
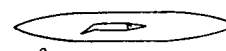
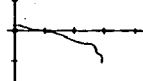
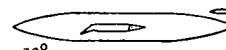

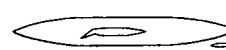


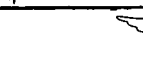
Span of L.E. Device (b/2)	Span of T.E. Device (b/2)	Configuration	$C_{L_{max}}$	$C_{L_{max}}$	L/D at $0.85 C_{L_{max}}$	C_m Characteristics	Figure
.75	T.E. Flaps	 $\delta_n = 10^\circ$ $\delta_f = 50^\circ$					16
		 $\delta_n = 20^\circ$.81	15.5	7.10		12
	 $\delta_n = 20^\circ$					17	
.35	T.E. Flaps	 $\delta_n = 20^\circ$ $\delta_f = 50^\circ$	1.10	14.9	4.82		12
		 $\delta_n = 20^\circ$ $\delta_f = 50^\circ$					17
.775	T.E. Flaps	 $\delta_n = 20^\circ$ $\delta_f = 50^\circ$	1.36	15.1	3.50		12
		 $\delta_n = 20^\circ$ $\delta_f = 50^\circ$					17
.775	L.E. Droop	 $\delta_n = 30^\circ$.87	16.6	6.84		13
		 $\delta_n = 30^\circ$					18 and 21
		$l/\bar{c} = 2$  $\delta_n = 30^\circ$ $i_t = -1.96^\circ$					21
		$l/\bar{c} = 2$  $\delta_n = 30^\circ$ $\frac{2z}{b} = .40$					21
		$l/\bar{c} = 2$  $\delta_n = 30^\circ$ $i_t = -1.75^\circ$					21
		$l/\bar{c} = 2$  $\delta_n = 30^\circ$ $\frac{2z}{b} = -.177$					21



TABLE III.- SUMMARY OF LONGITUDINAL STABILITY CHARACTERISTICS OF AN UNSWEPT WING HAVING THIN HEXAGONAL AIRFOIL SECTIONS AND AN ASPECT RATIO OF 2.5 - Continued


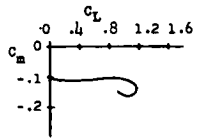

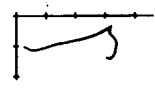

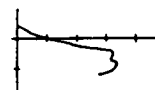
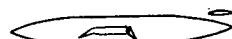

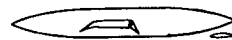

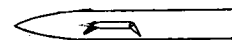
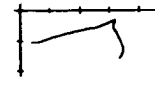



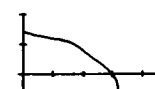

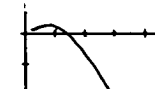

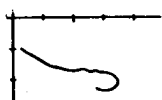
Span of L.E. Device (b/2)	Span of T.E. Device (b/2)	Configuration	$C_{L_{max}}$	$^a C_{L_{max}}$	L/D at $0.85 C_{L_{max}}$	C_m Characteristics	Figure
.775 L.E. Droop	.35 T.E. Flaps	 $\delta_n = 30^\circ$ $\delta_f = 50^\circ$	1.17	16.2	4.52		13
		 $\delta_n = 30^\circ$ $\delta_f = 50^\circ$					18 and 22(a)
		 $1/\bar{c} = 2$ $\delta_n = 30^\circ$ $\delta_f = 50^\circ$ $\frac{2x}{b} = .40$ $i_t = -1.96^\circ$					22(a)
		 $1/\bar{c} = 2$ $\delta_n = 30^\circ$ $\delta_f = 50^\circ$ $\frac{2x}{b} = .177$ $i_t = -1.75^\circ$					22(a)
		 $1/\bar{c} = 2$ $\delta_n = 30^\circ$ $\delta_f = 50^\circ$ $\frac{2x}{b} = -.177$ $i_t = -2.11^\circ$					22(a)
.775 L.E. Droop	.35 T.E. Flaps	 $\delta_n = 30^\circ$ $\delta_f = 50^\circ$					22(b)
		 $1/\bar{c} = 3$ $\delta_n = 30^\circ$ $\delta_f = 50^\circ$ $\frac{2x}{b} = .40$ $i_t = -1.98^\circ$					22(b)
		 $1/\bar{c} = 3$ $\delta_n = 30^\circ$ $\delta_f = 50^\circ$ $\frac{2x}{b} = .177$ $i_t = -1.70^\circ$					22(b)
		 $1/\bar{c} = 3$ $\delta_n = 30^\circ$ $\delta_f = 50^\circ$ $\frac{2x}{b} = -.177$ $i_t = -2.10^\circ$					22(b)
.775 L.E. Droop	.75 T.E. Flaps	 $\delta_n = 30^\circ$ $\delta_f = 50^\circ$	1.39	16.3	3.81		13



TABLE III.- SUMMARY OF LONGITUDINAL STABILITY CHARACTERISTICS OF AN UNSWEPT WING HAVING THIN HEXAGONAL AIRFOIL SECTIONS AND AN ASPECT RATIO OF 2.5 - Continued

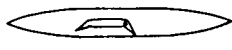
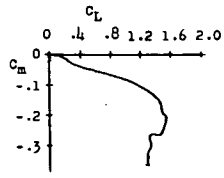
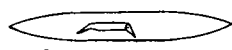
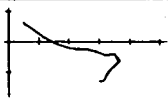
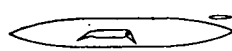



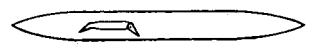
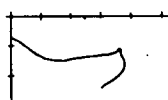
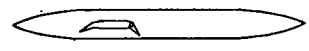
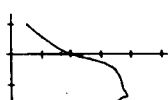
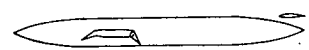
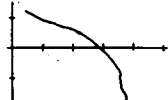
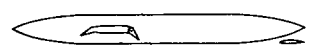
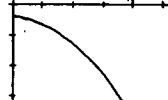
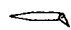
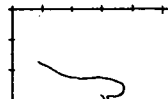
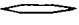
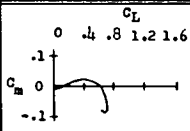
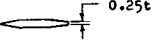
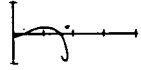

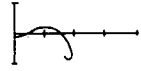
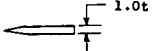
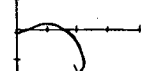
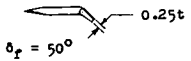
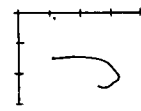
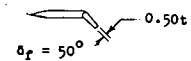
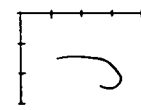
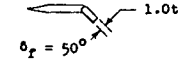
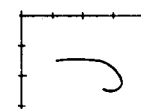
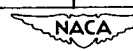
Span of L.E. Device (b/2)	Span of T.E. Device (b/2)	Configuration	$C_{l_{max}}$	$a_{C_{l_{max}}}$	L/D at $0.85 C_{l_{max}}$	C_m Characteristics	Figure
.775 L.E. Droop	.75 T.E. Flaps	 $\delta_n = 30^\circ$ $\delta_f = 50^\circ$					18 and 23(a)
		$l/\bar{c} = 2$ $\frac{2x}{b} = .40$  $\delta_n = 30^\circ$ $i_t = -3.96^\circ$ $\delta_f = 50^\circ$					23(a)
		$l/\bar{c} = 2$ $\frac{2x}{b} = .177$  $\delta_n = 30^\circ$ $i_t = -1.70^\circ$ $\delta_f = 50^\circ$					23(a)
		$l/\bar{c} = 2$ $\frac{2x}{b} = -.177$  $\delta_n = 30^\circ$ $i_t = -2.14^\circ$ $\delta_f = 50^\circ$					23(a)
		 $\delta_n = 30^\circ$ $\delta_f = 50^\circ$					23(b)
		$l/\bar{c} = 3$ $\frac{2x}{b} = .40$  $\delta_n = 30^\circ$ $i_t = -1.88^\circ$ $\delta_f = 50^\circ$					23(b)
		$l/\bar{c} = 3$ $\frac{2x}{b} = .177$  $\delta_n = 30^\circ$ $i_t = -1.68^\circ$ $\delta_f = 50^\circ$					23(b)
		$l/\bar{c} = 3$ $\frac{2x}{b} = -.177$  $\delta_n = 30^\circ$ $i_t = -2.12^\circ$ $\delta_f = 50^\circ$					23(b)
None	1.00 T.E. Flaps	 $\delta_f = 50^\circ$					Un-published



TABLE III.- SUMMARY OF LONGITUDINAL STABILITY CHARACTERISTICS OF AN UNSWEPT WING HAVING THIN HEXAGONAL AIRFOIL SECTIONS AND AN ASPECT RATIO OF 2.5 - Concluded

Span of L.E. Device (b/2)	Span of T.E. Device (b/2)	Configuration	$C_{l_{max}}$	$a_{C_{l_{max}}}$	L/D at $0.85 C_{l_{max}}$	C_m Characteristics		
None	None	 Wing tips of elliptical cross section	0.70	13.8	5.08		6	
			.73	14.3	5.08		5	
			.76	14.7	4.92			
		.83	14.5	4.7				
	.75 T.E. flaps	None	 $\delta_f = 50^\circ$	1.30	12.2	3.50		9
			 $\delta_f = 50^\circ$	1.33	12.3	3.42		
			 $\delta_f = 50^\circ$	1.33	12.2	3.34		



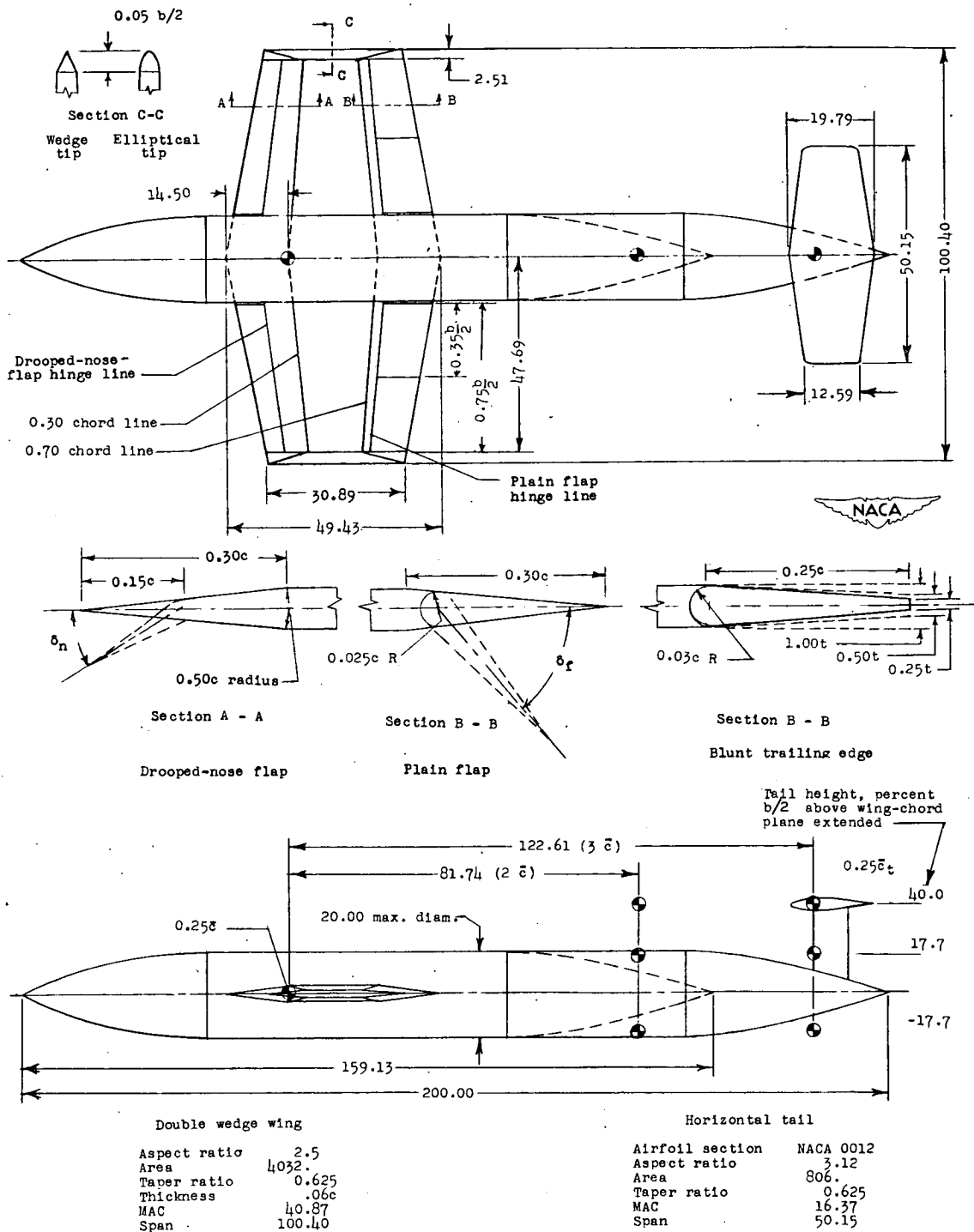
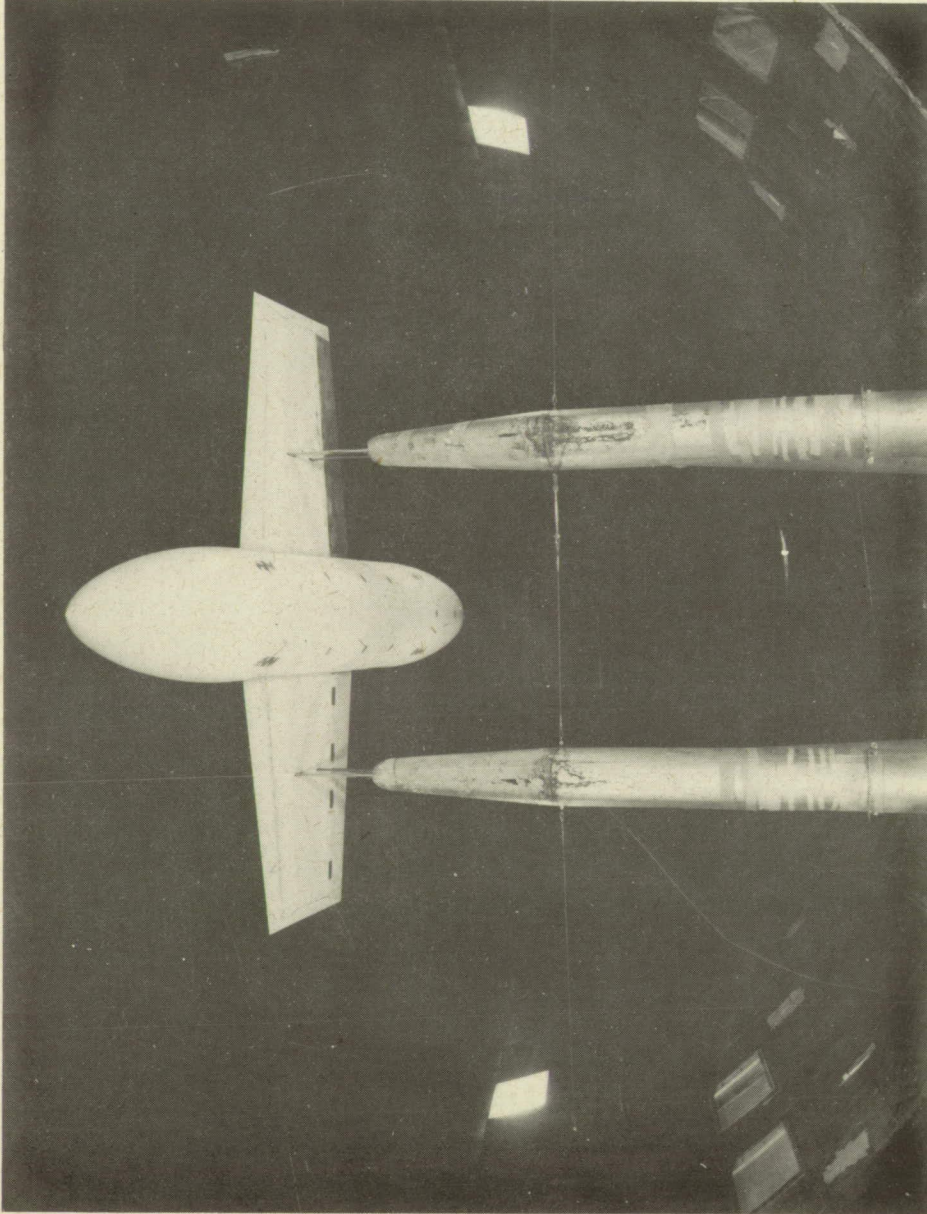


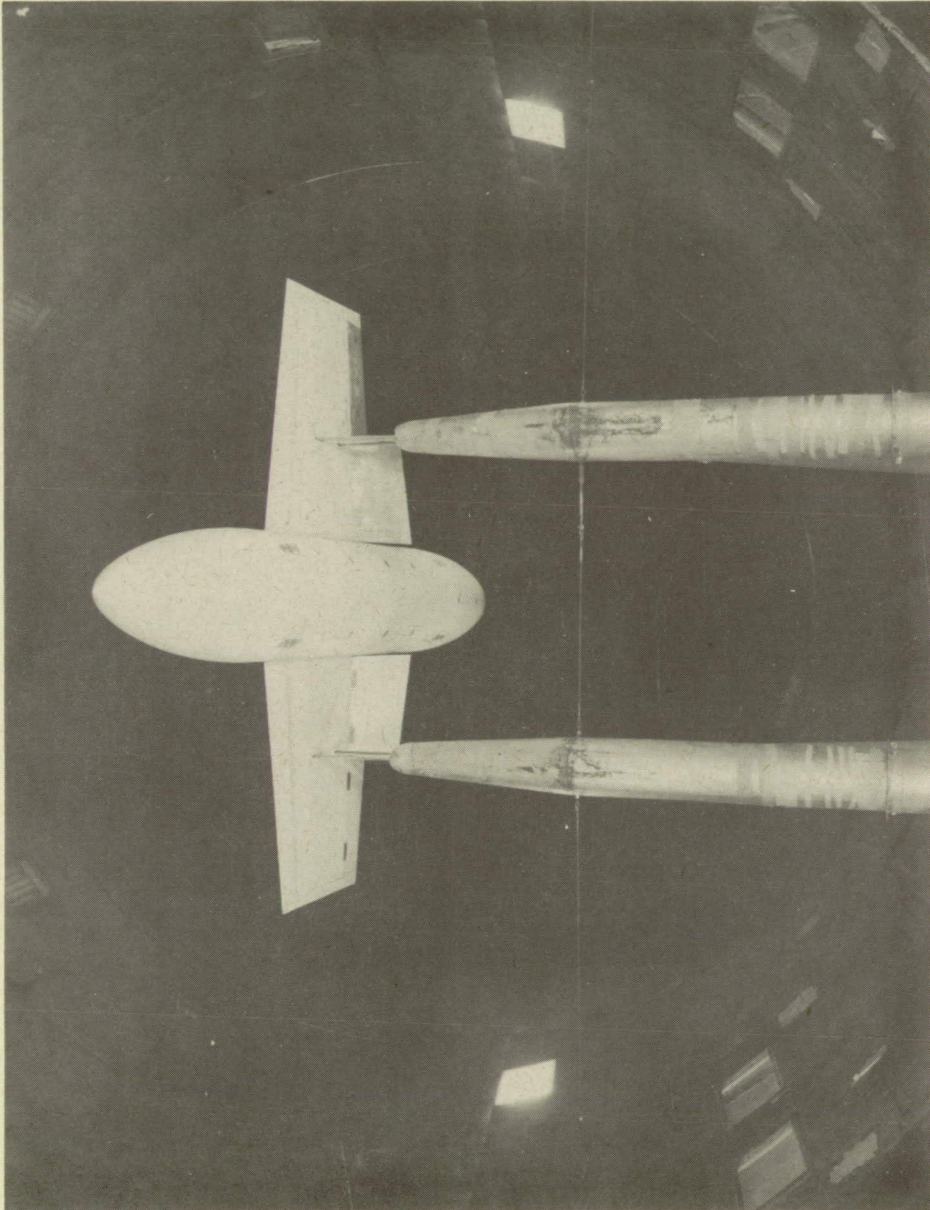
Figure 1- Geometry of wing, fuselage, and horizontal tail. All dimensions are in inches except as noted.



NACA
L-62212

(a) Plain wing.

Figure 2.-- Front view of wing-fuselage combination as mounted in the Langley 19-foot pressure tunnel.



(b) 0.35b plain flaps.

Figure 2.- Continued.

NACA
L-63241




(c) Drooped-nose flaps and 0.75b plain flaps.  L-76929

Figure 2.- Concluded.

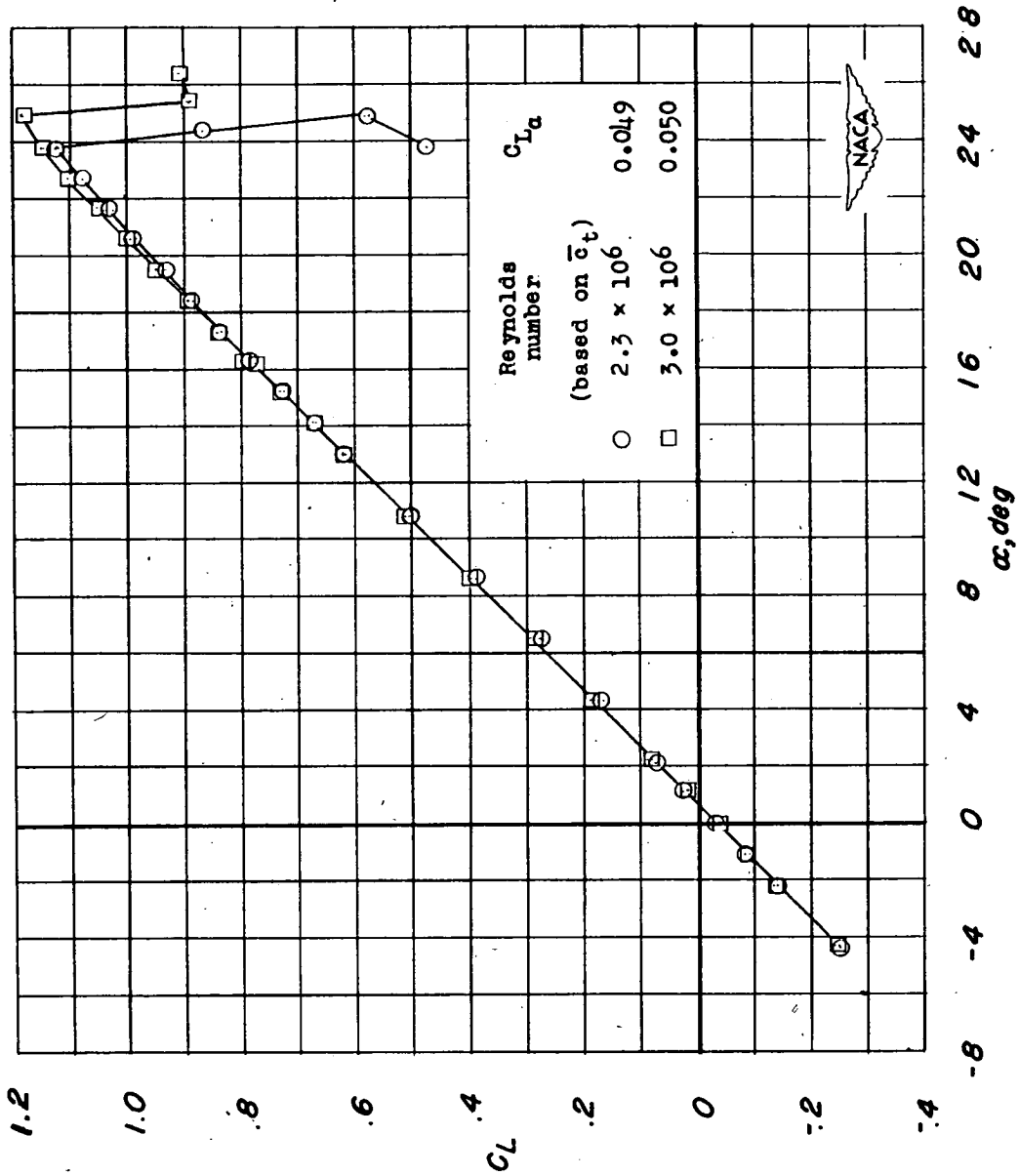


Figure 3.- Variation of lift coefficient with angle of attack of horizontal tail having an aspect ratio of 3.12 and NACA 0012 airfoil sections.

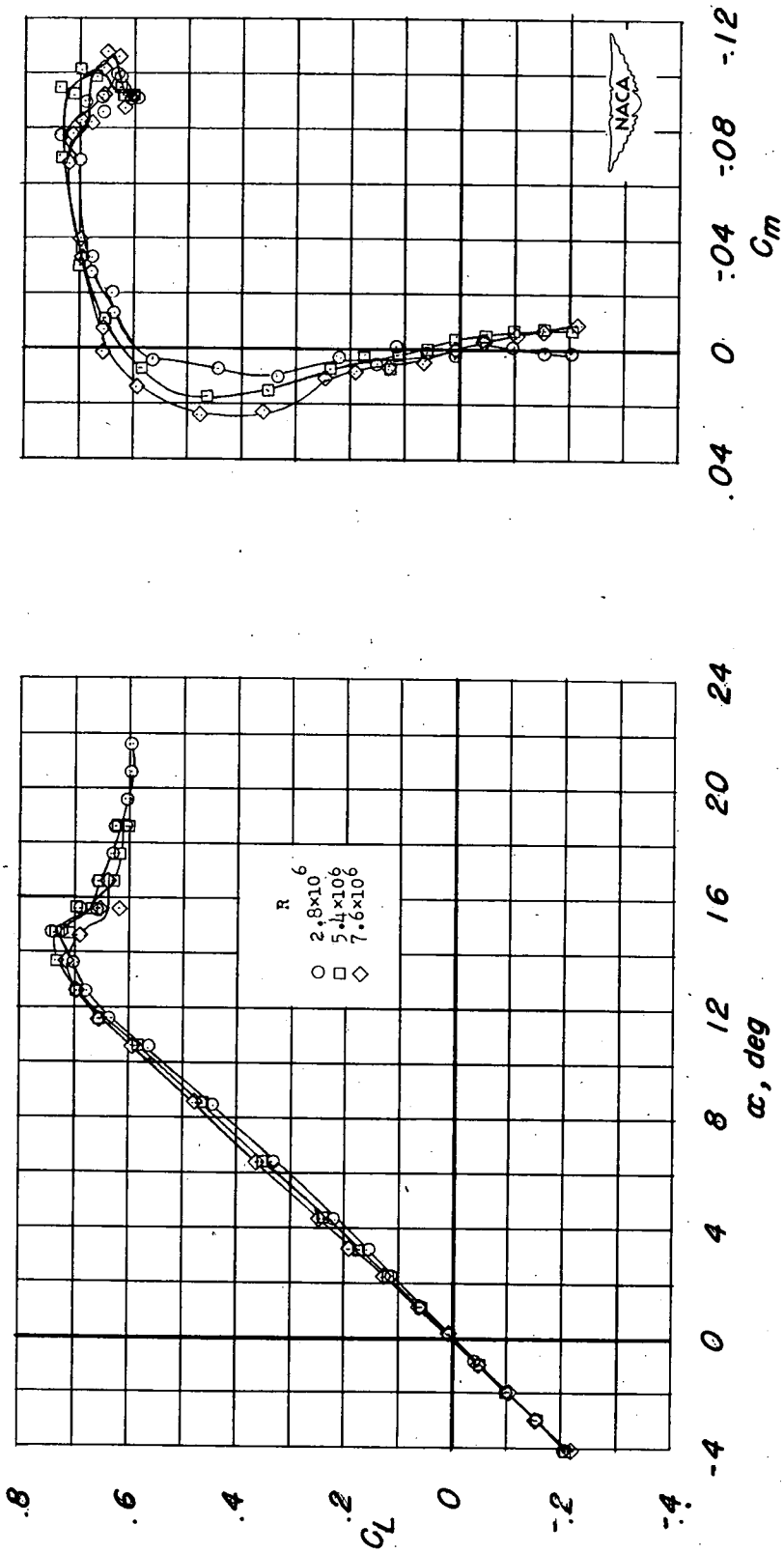


Figure 4.- Effect of Reynolds number on the lift, drag, and pitching-moment characteristics of the plain wing.

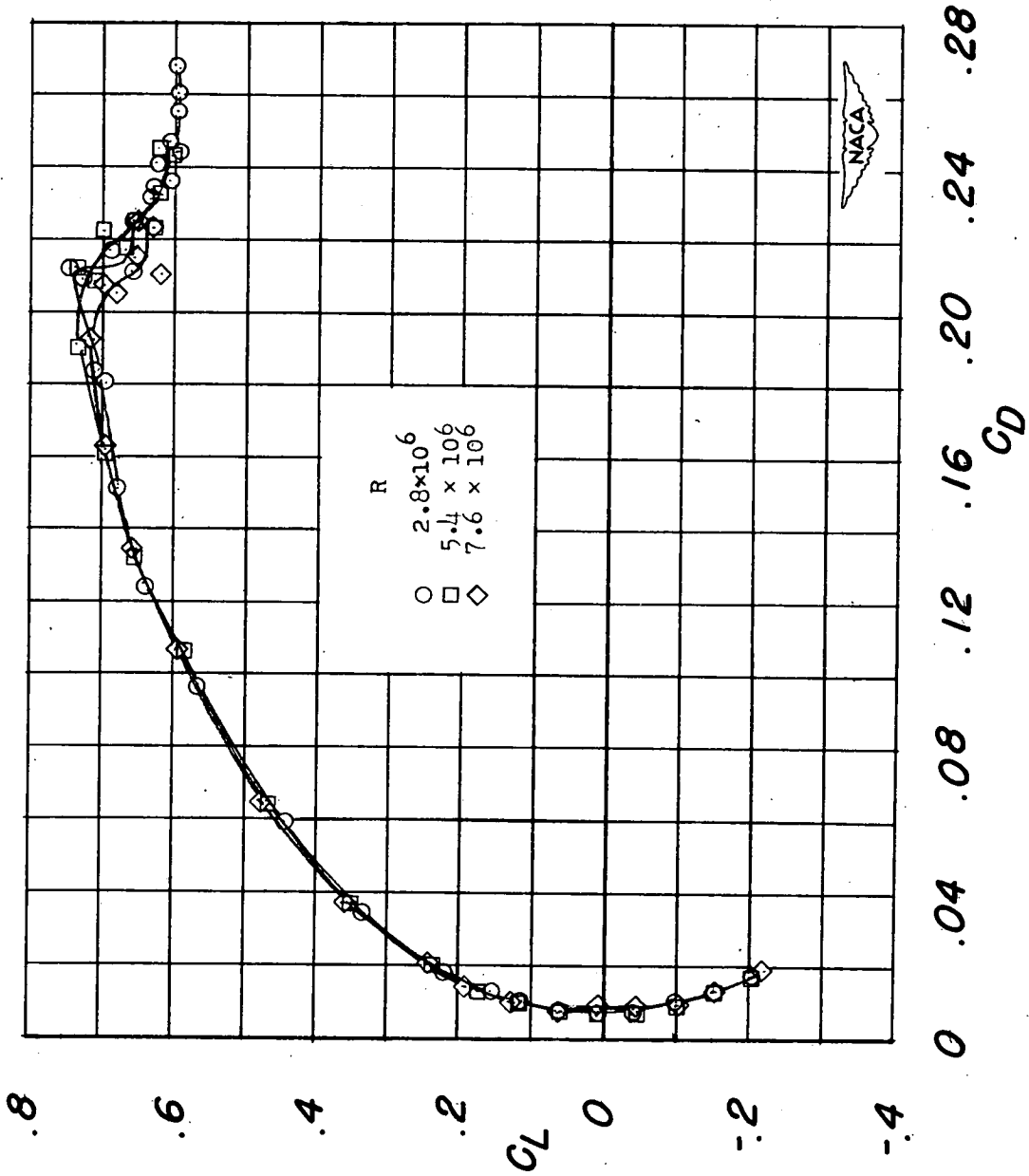


Figure 4.- Concluded.

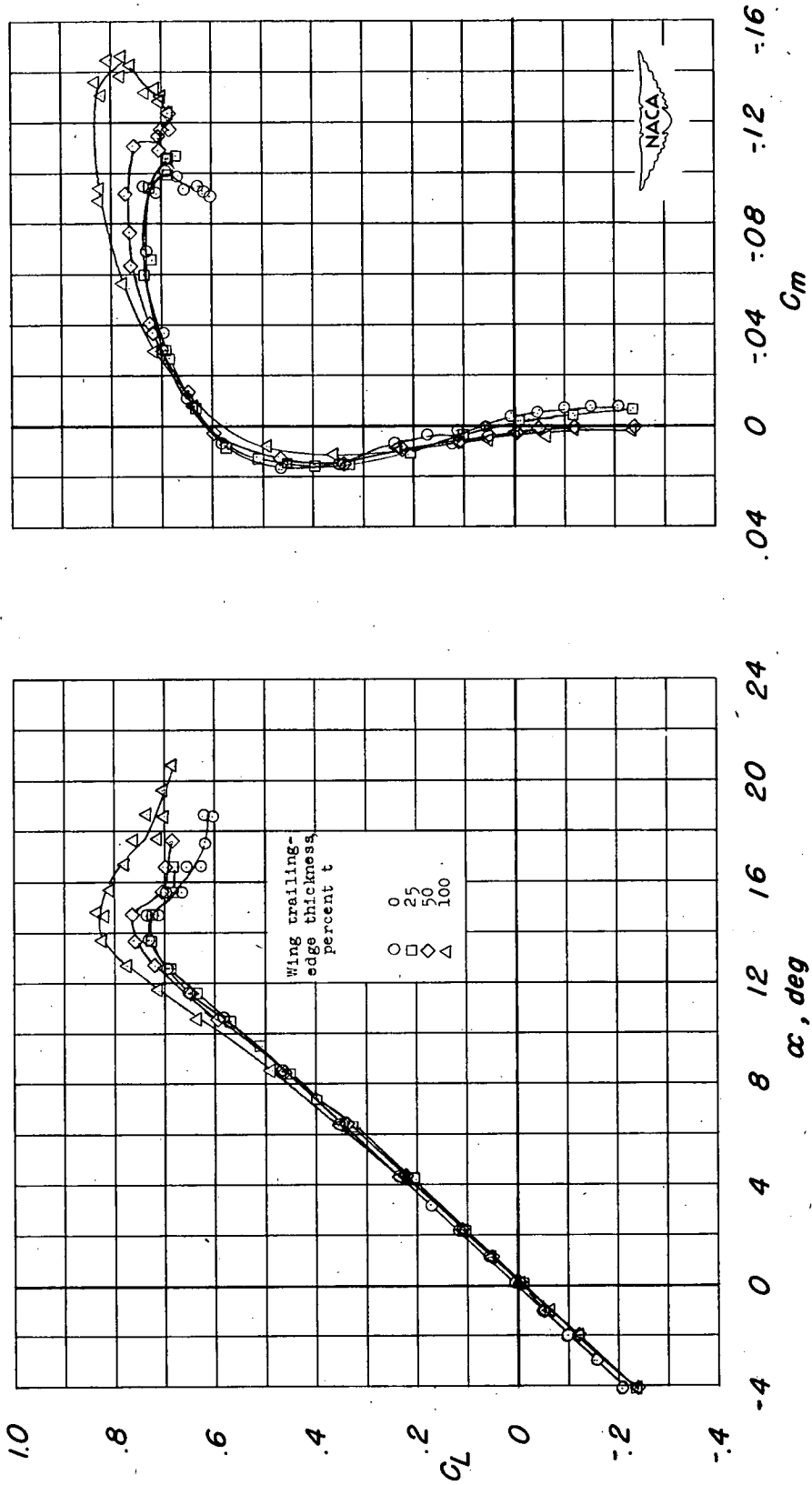


Figure 5.- Effect of trailing-edge thickness on the lift, drag, and pitching-moment characteristics of the plain wing. $R = 5.4 \times 10^6$.

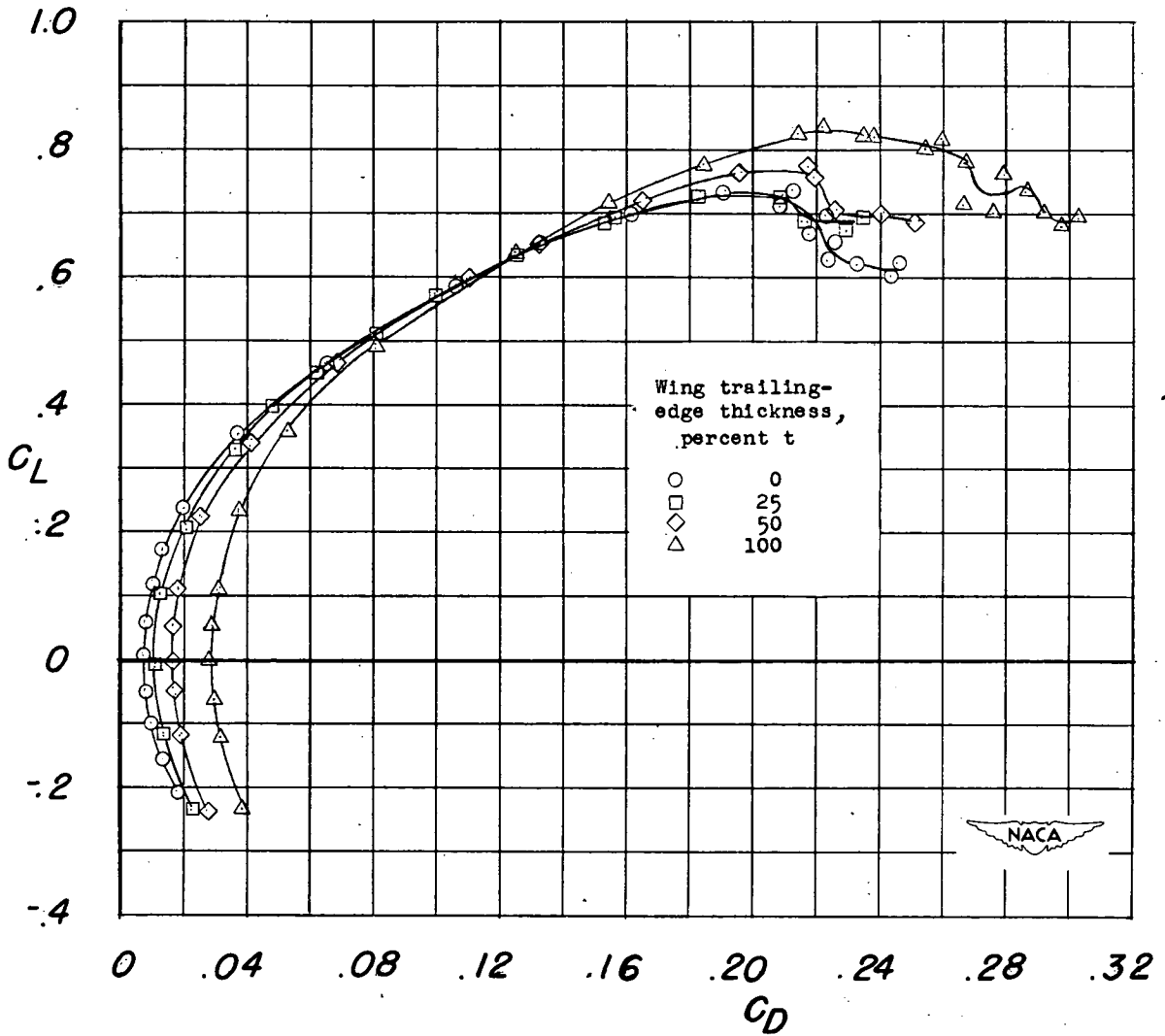


Figure 5.- Concluded.

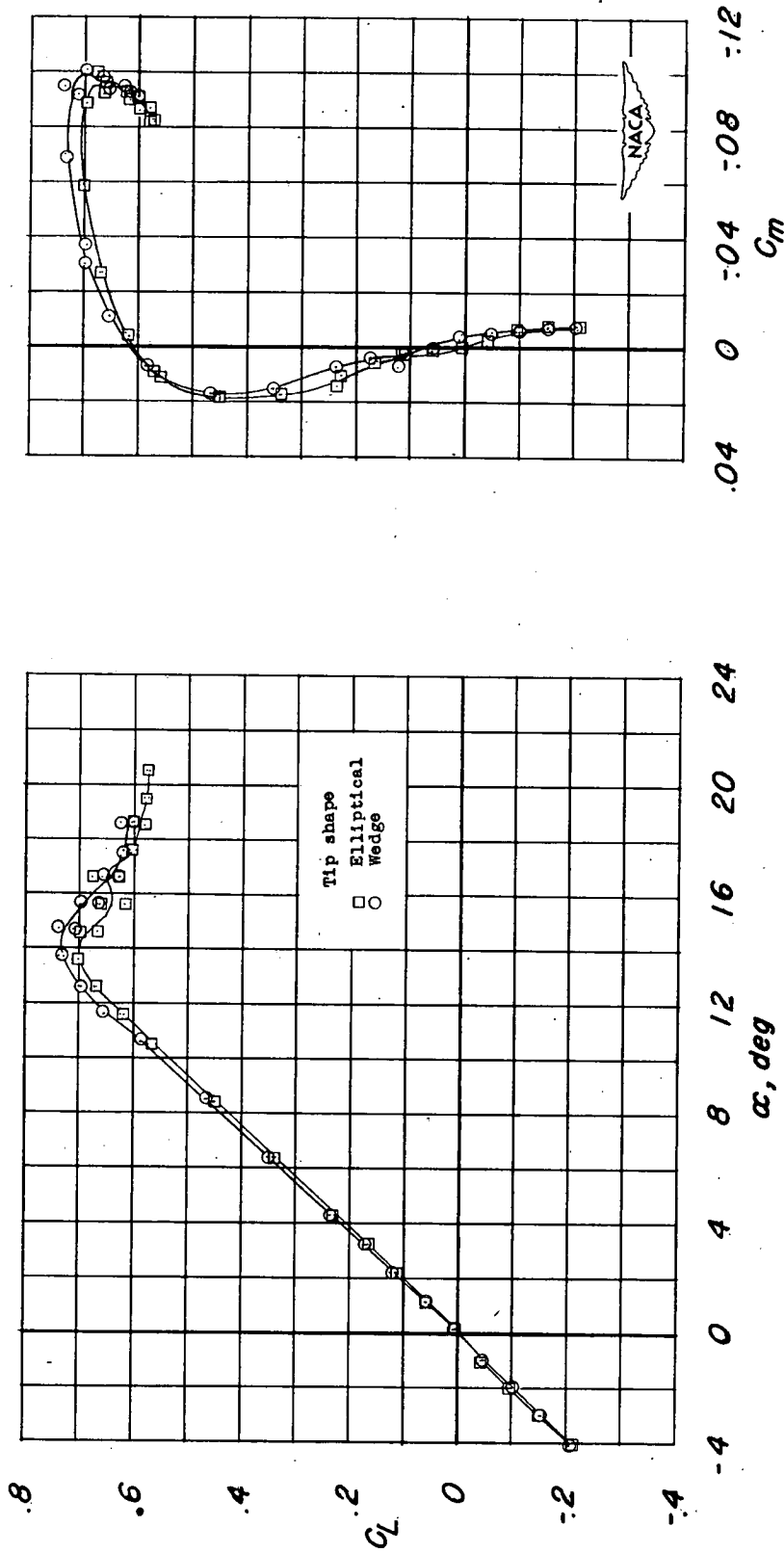


Figure 6.- Effect of tip shape on the lift, drag, and pitching-moment characteristics of the plain wing. $R = 5.4 \times 10^6$.

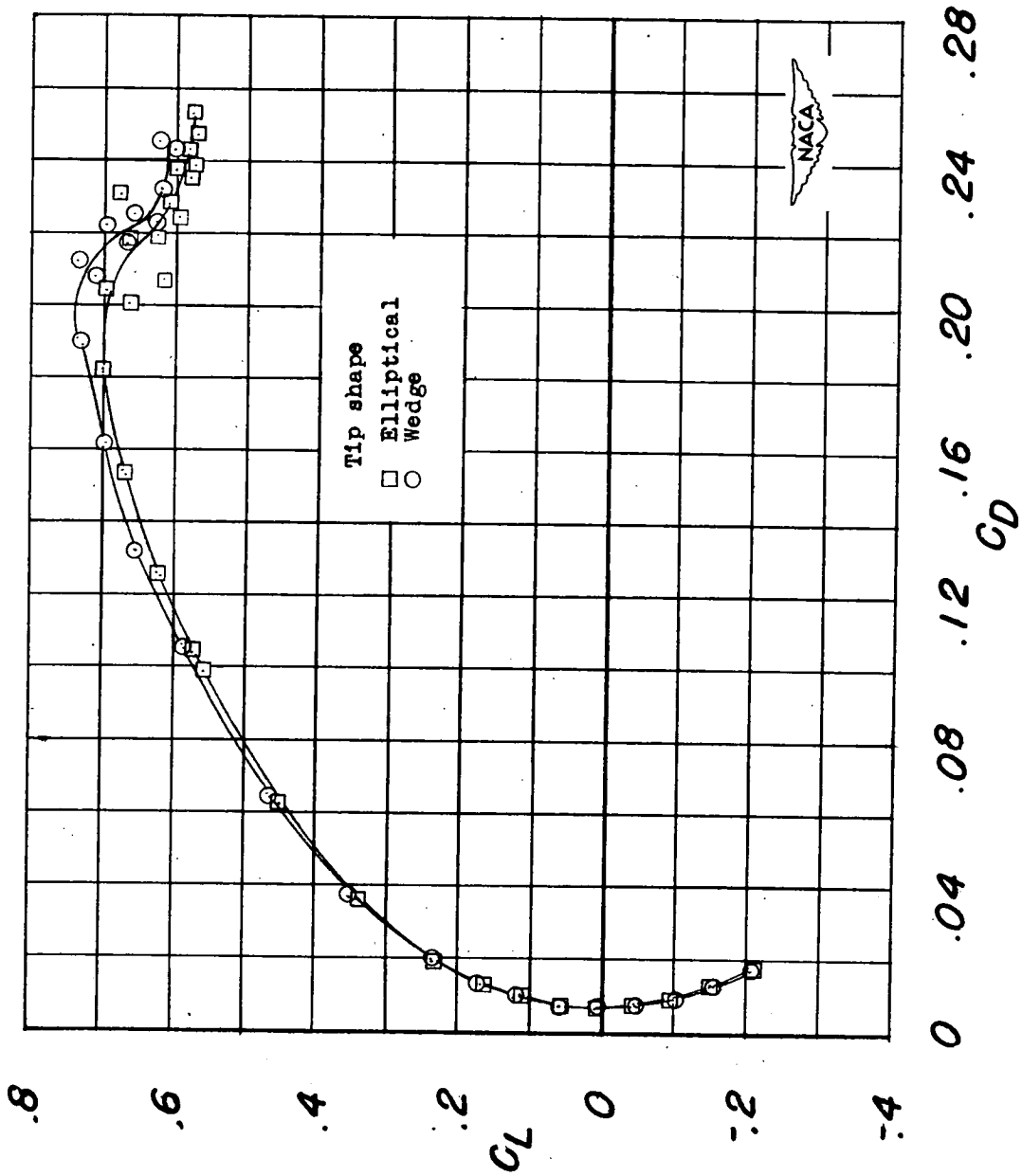


Figure 6.- Concluded.

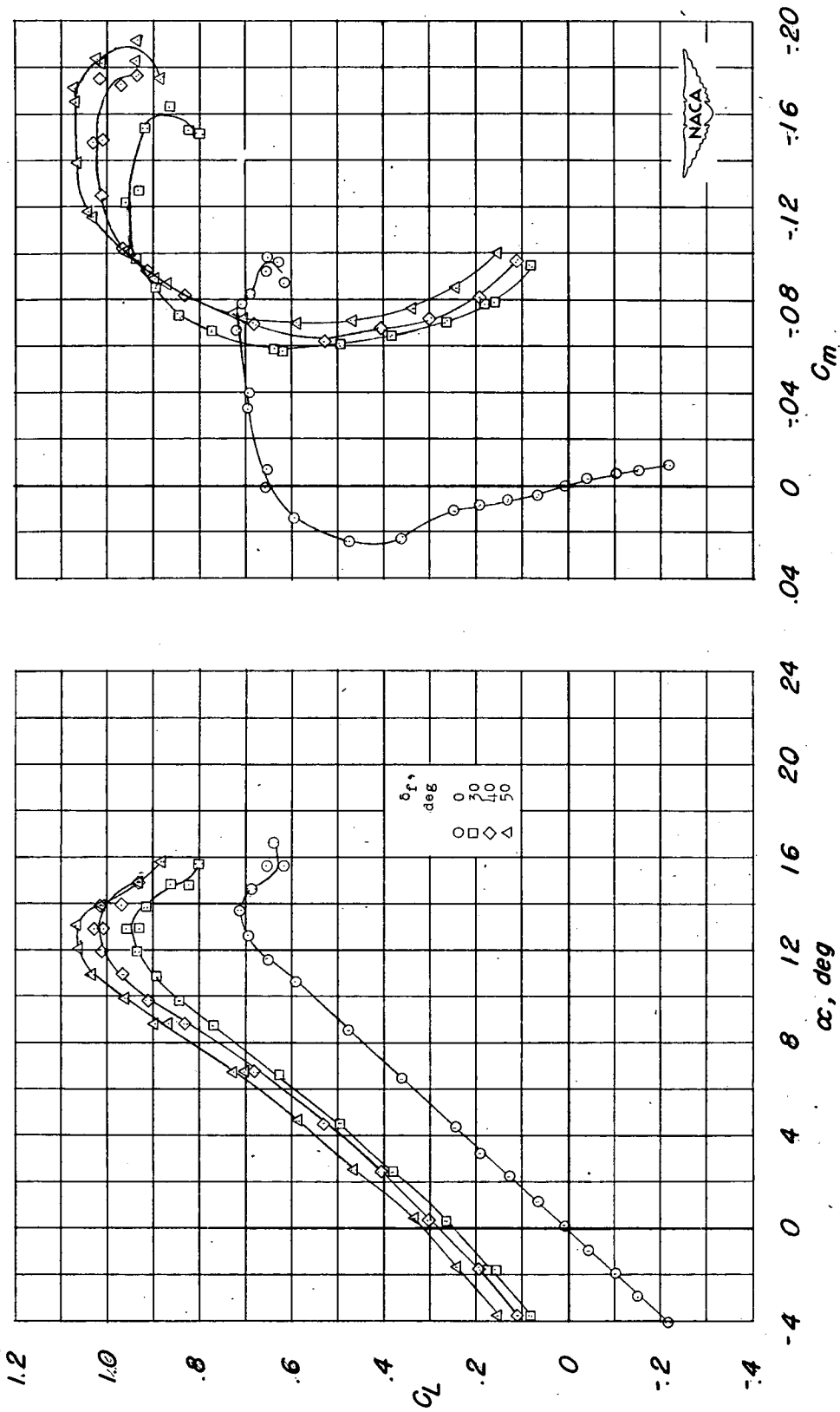


Figure 7.- Effect of deflection of 0.35b plain flaps on the lift, drag, and pitching-moment characteristics of the wing. $R = 7.6 \times 10^6$.

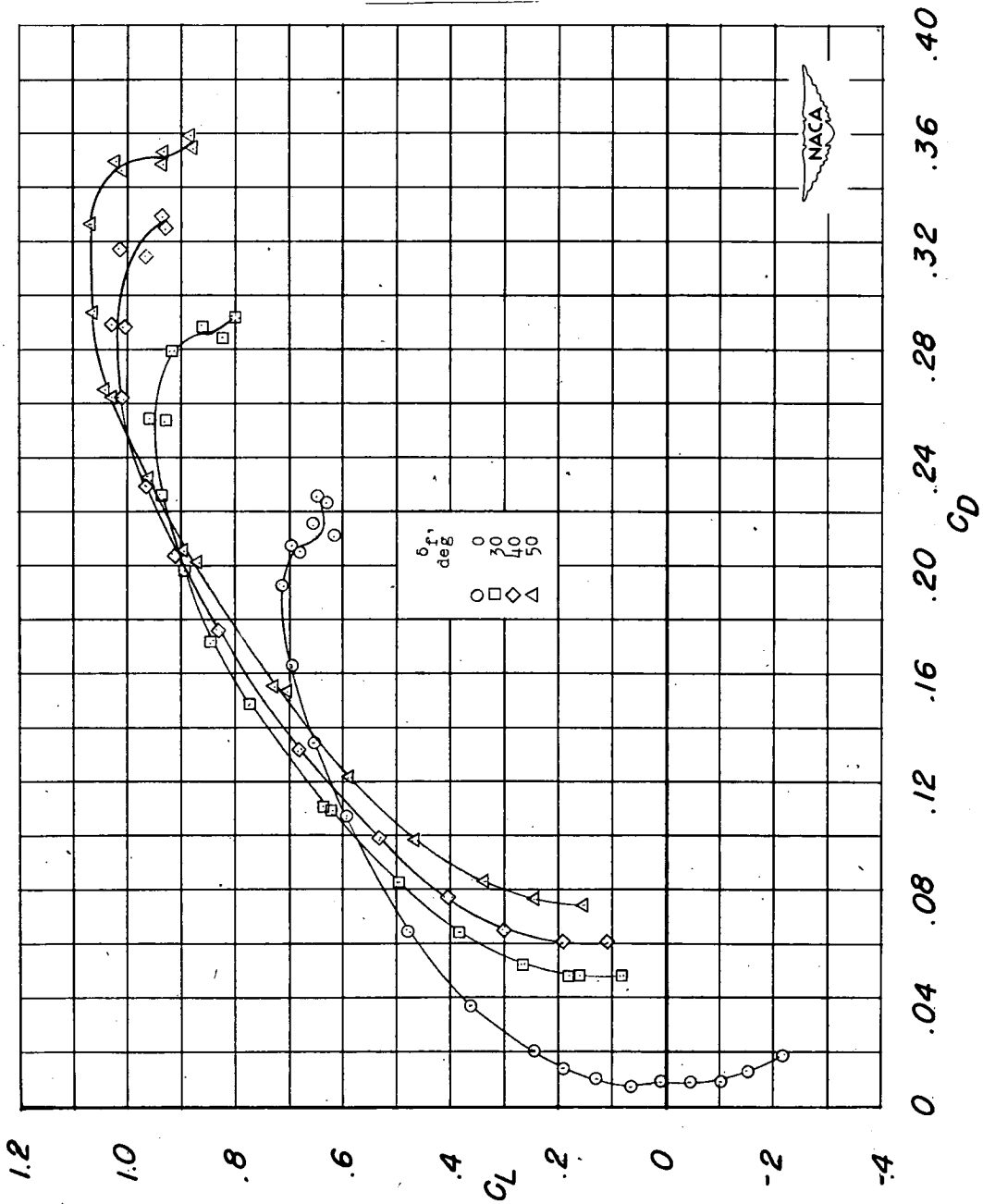


Figure 7.- Concluded.

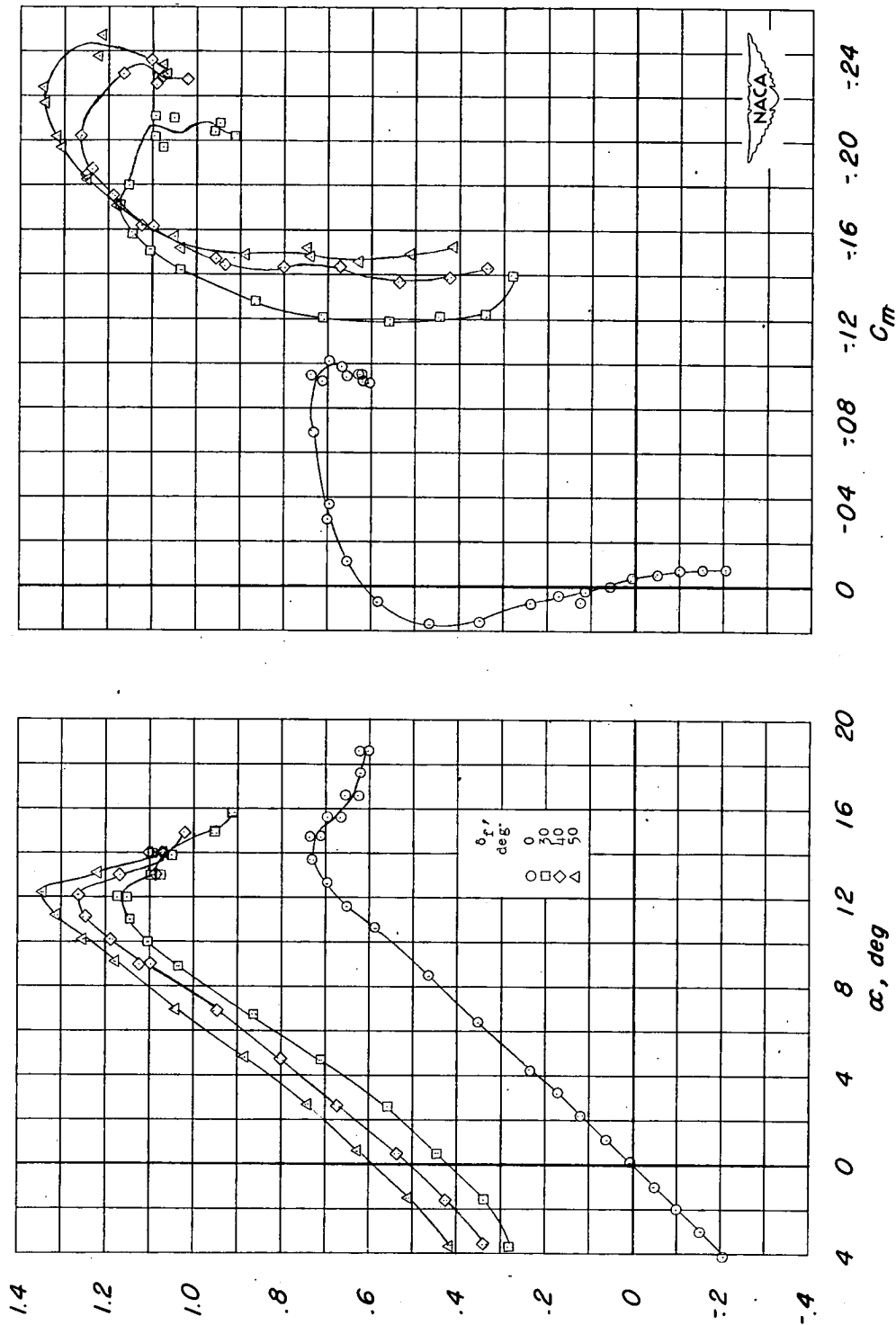


Figure 8.- Effect of deflection of 0.75b plain flaps on the lift, drag, and pitching-moment characteristics of the wing. $R = 5.4 \times 10^6$.

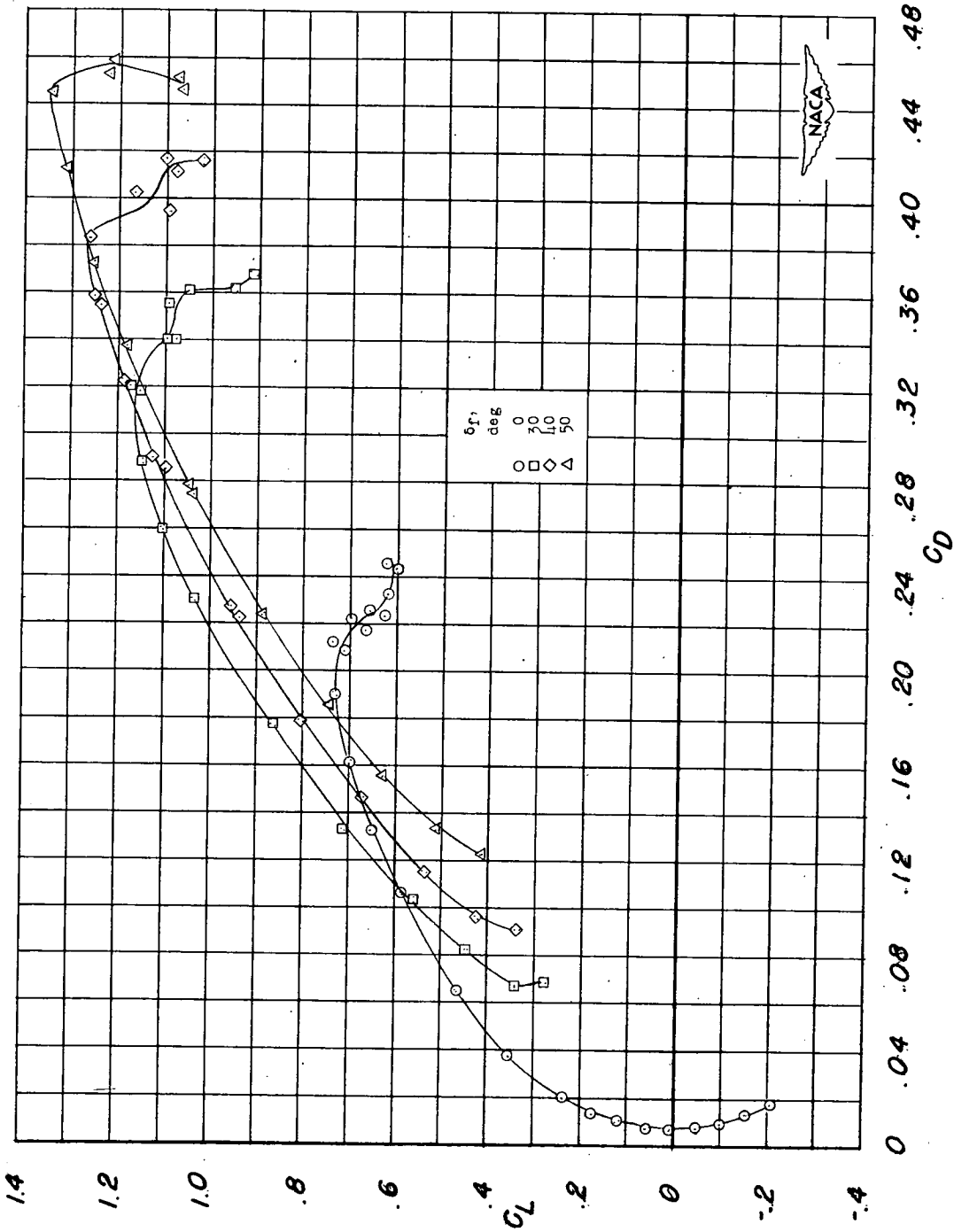


Figure 8.- Concluded.

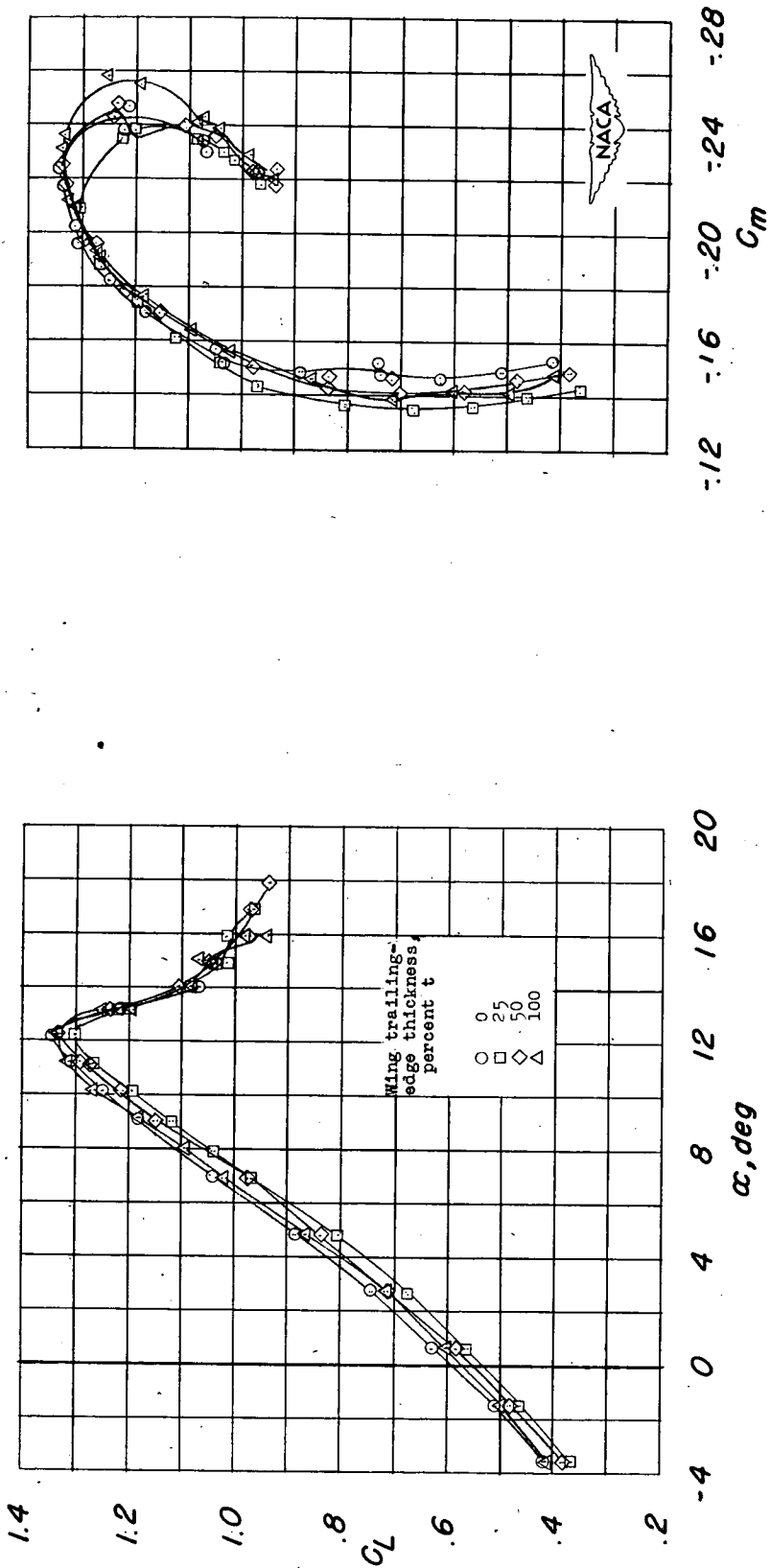


Figure 9.- Effect of trailing-edge thickness on the lift, drag, and pitching-moment characteristics of the wing with 0.75b plain flap deflected 50° . $R = 5.4 \times 10^6$.

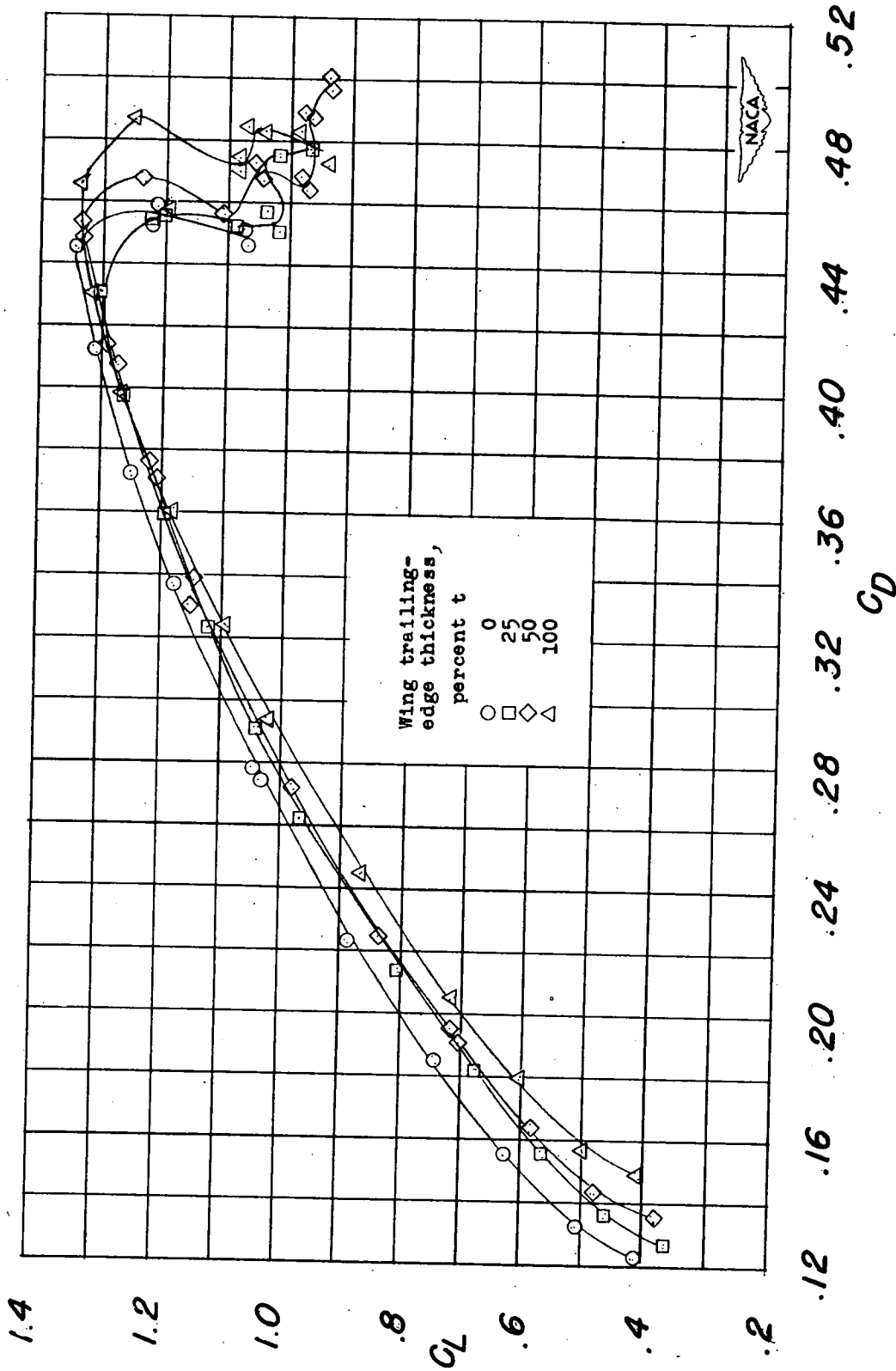


Figure 9.- Concluded.

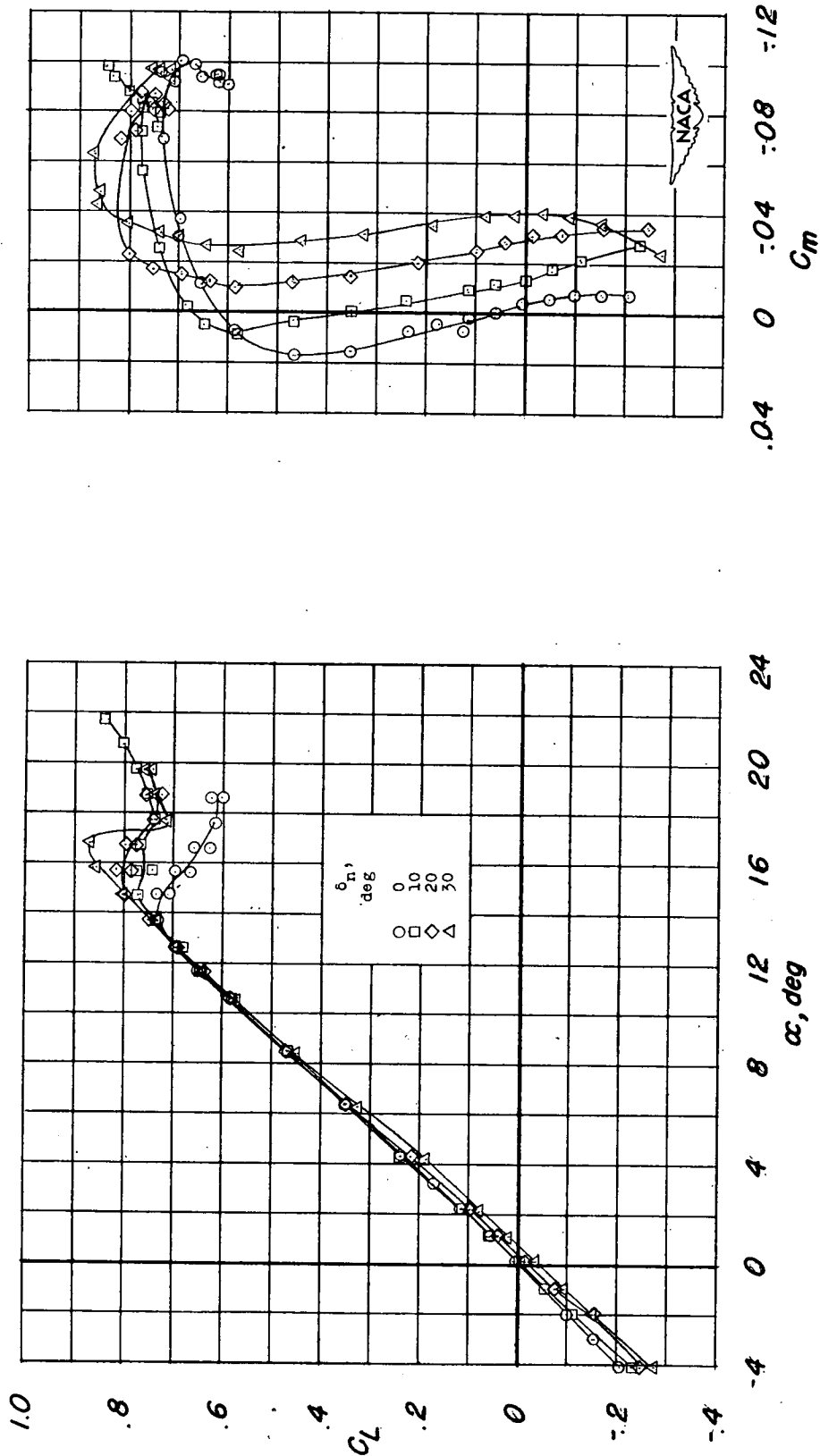


Figure 10.- Effect of drooped-nose-flap deflection on lift, drag, and pitching moment of the wing. $R = 7.6 \times 10^6$.

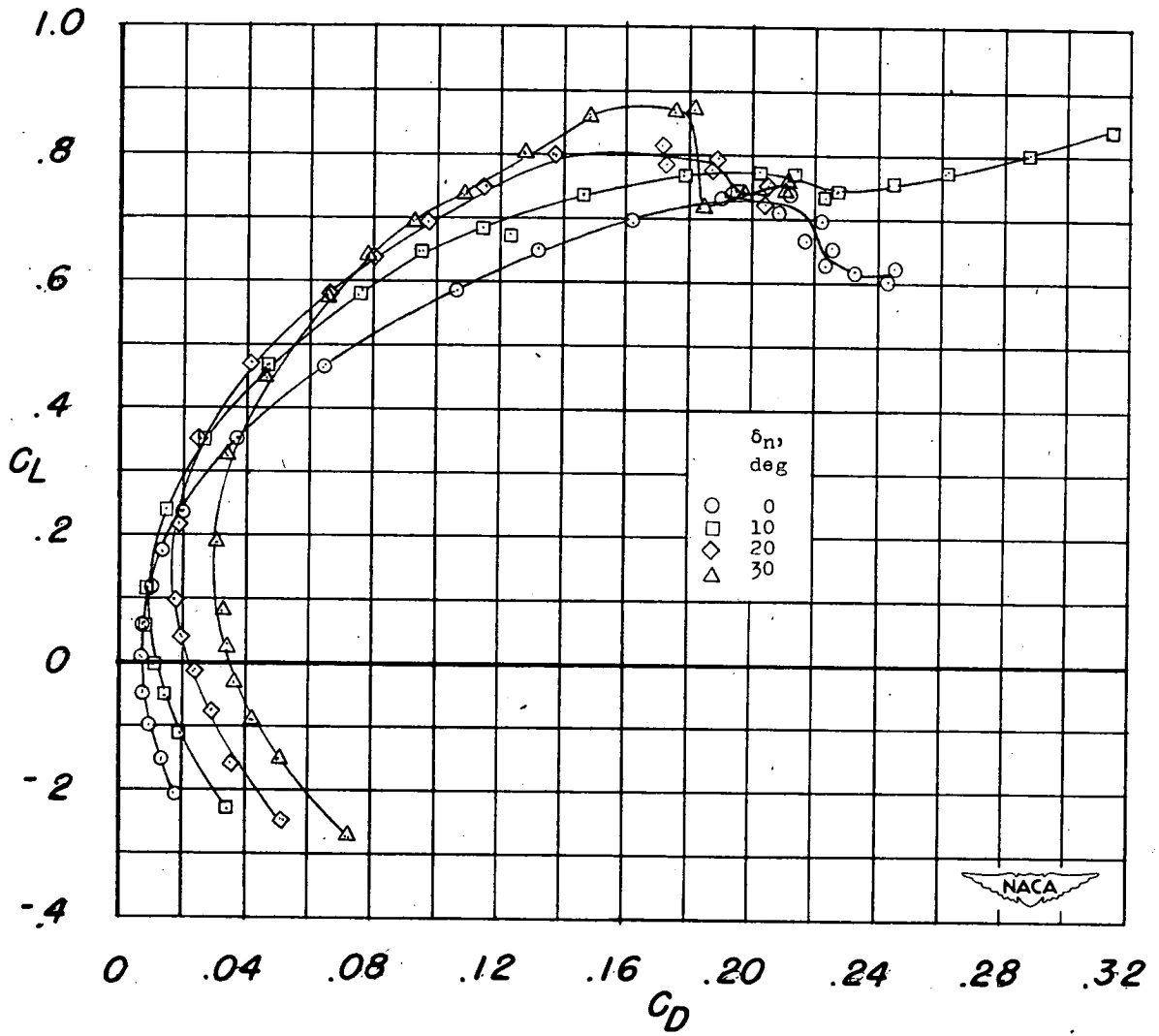


Figure 10.- Concluded.

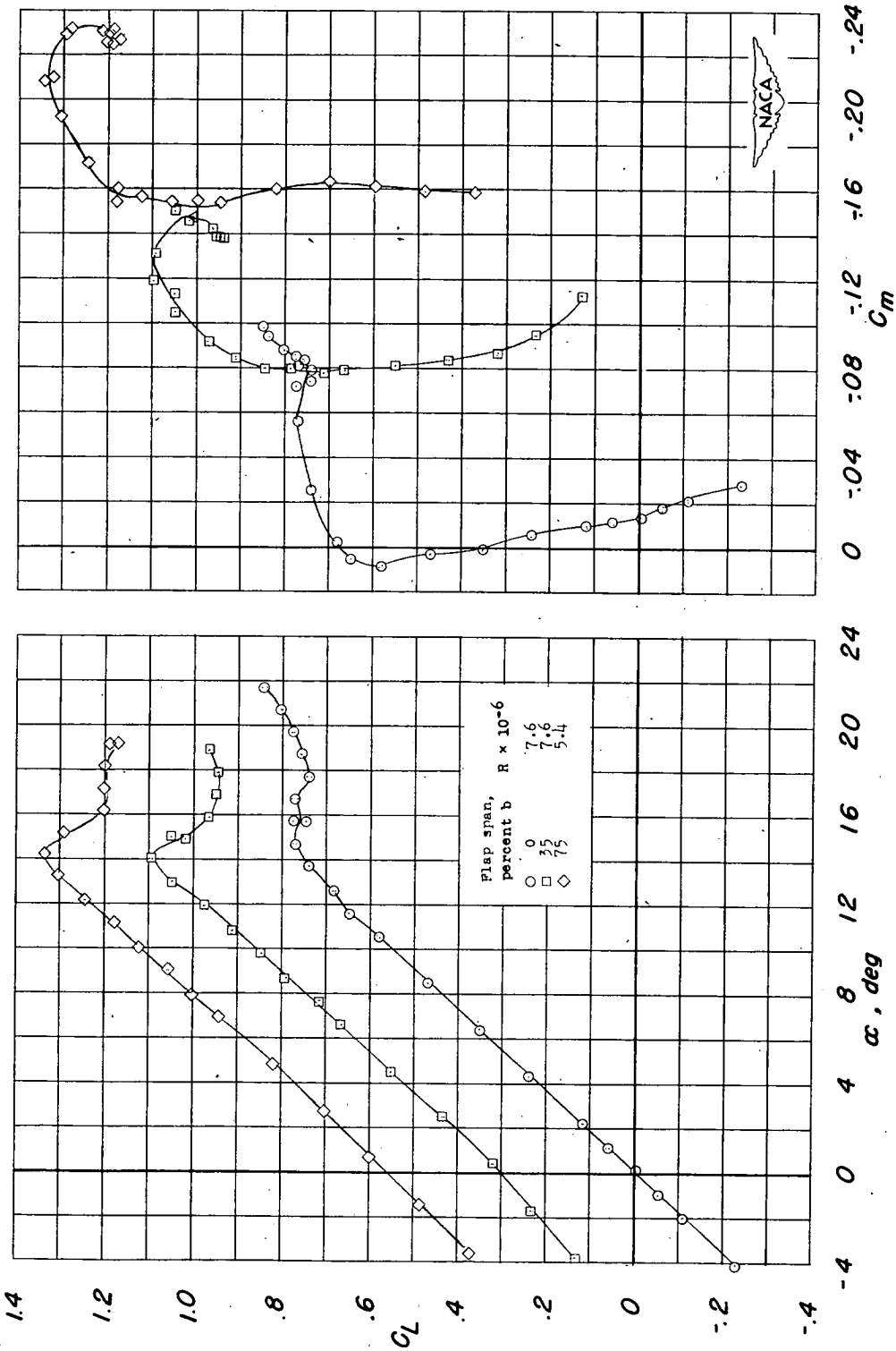


Figure 11.- Effect of plain flap span on the lift, drag, and pitching-moment characteristics of the wing with drooped-nose flaps deflected 10° . $\delta_f = 50^\circ$.

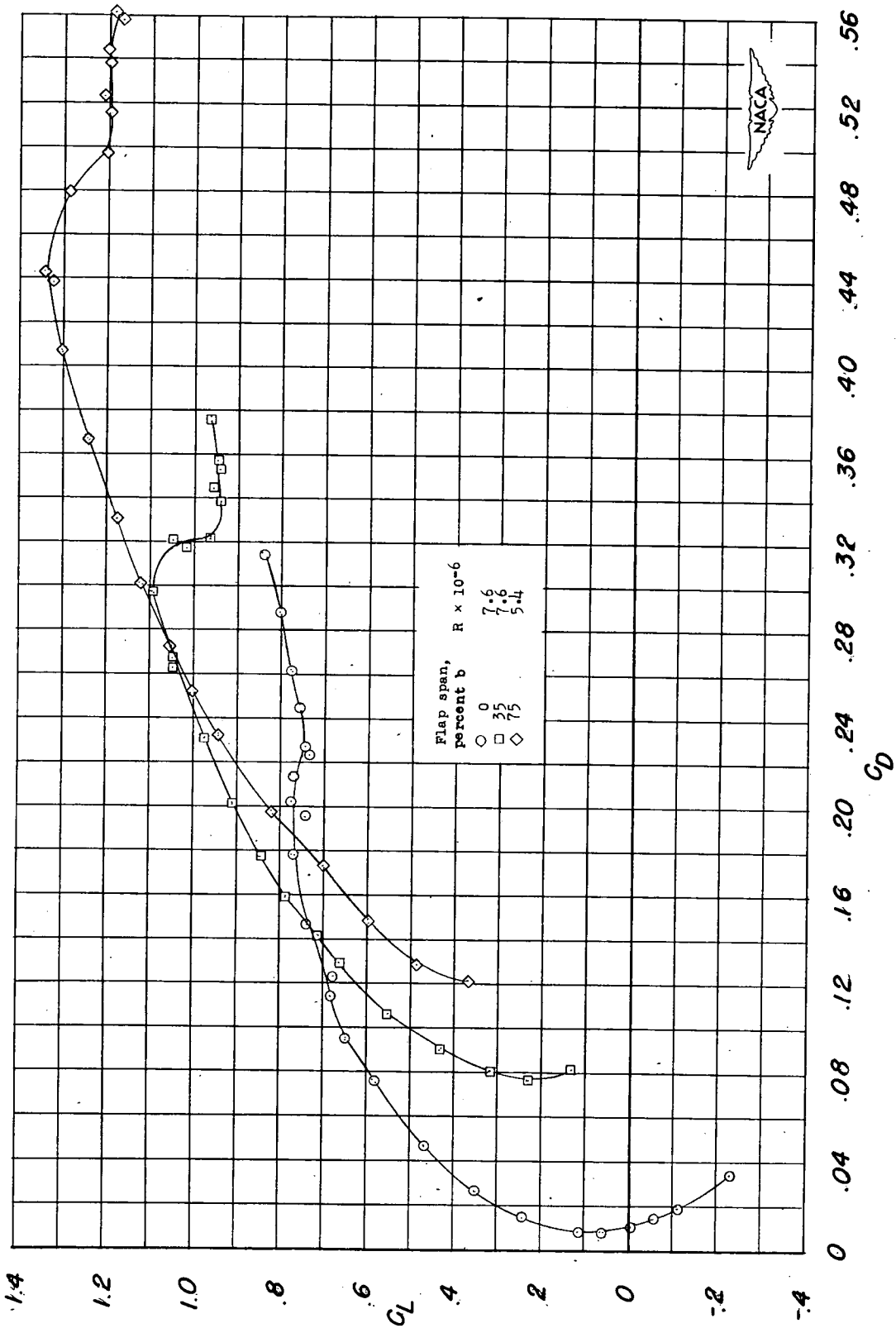


Figure 11.- Concluded.

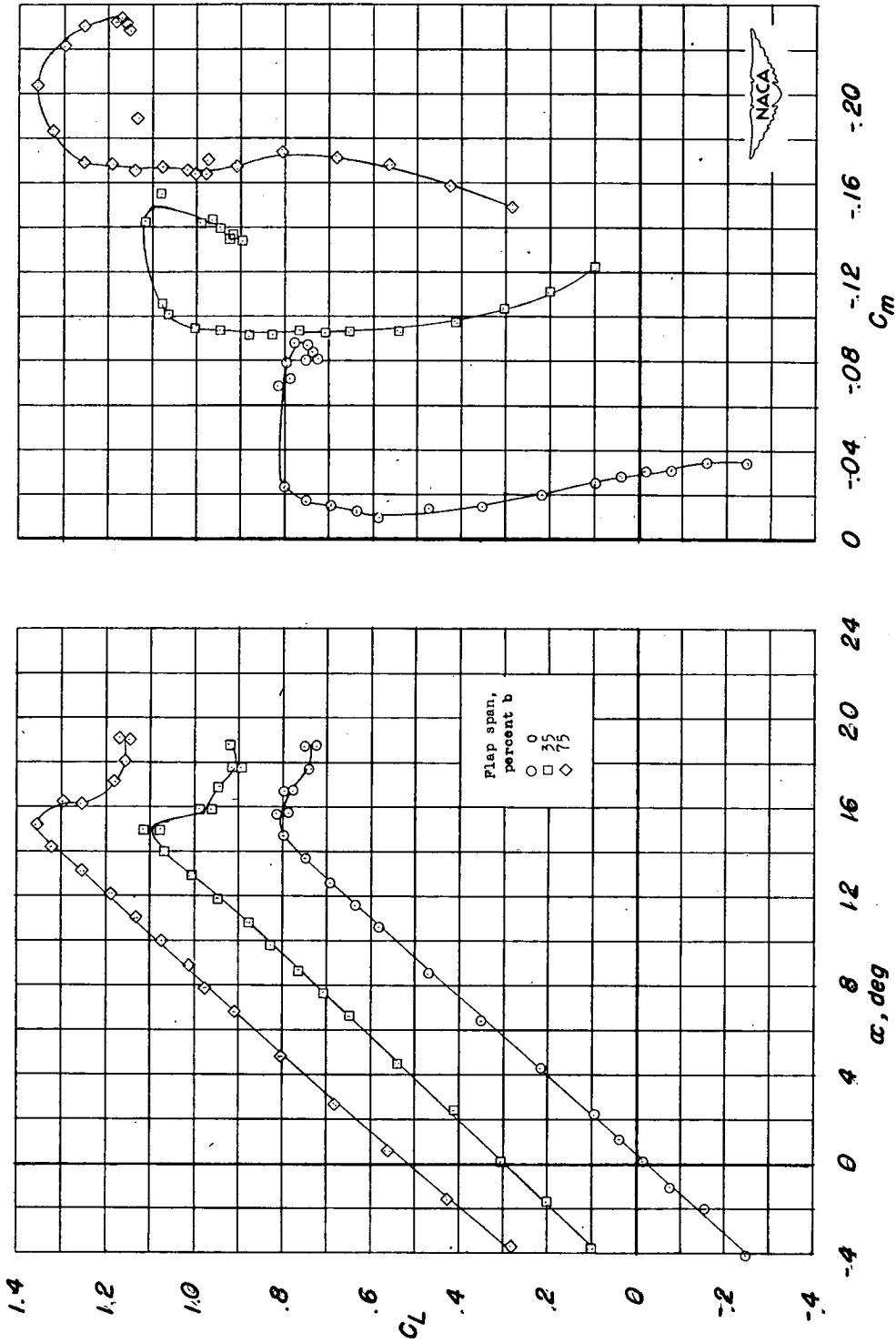


Figure 12.- Effect of plain flap span on the lift, drag, and pitching-moment characteristics of the wing with drooped-nose flaps deflected 20° . $\delta_F = 50^\circ$.

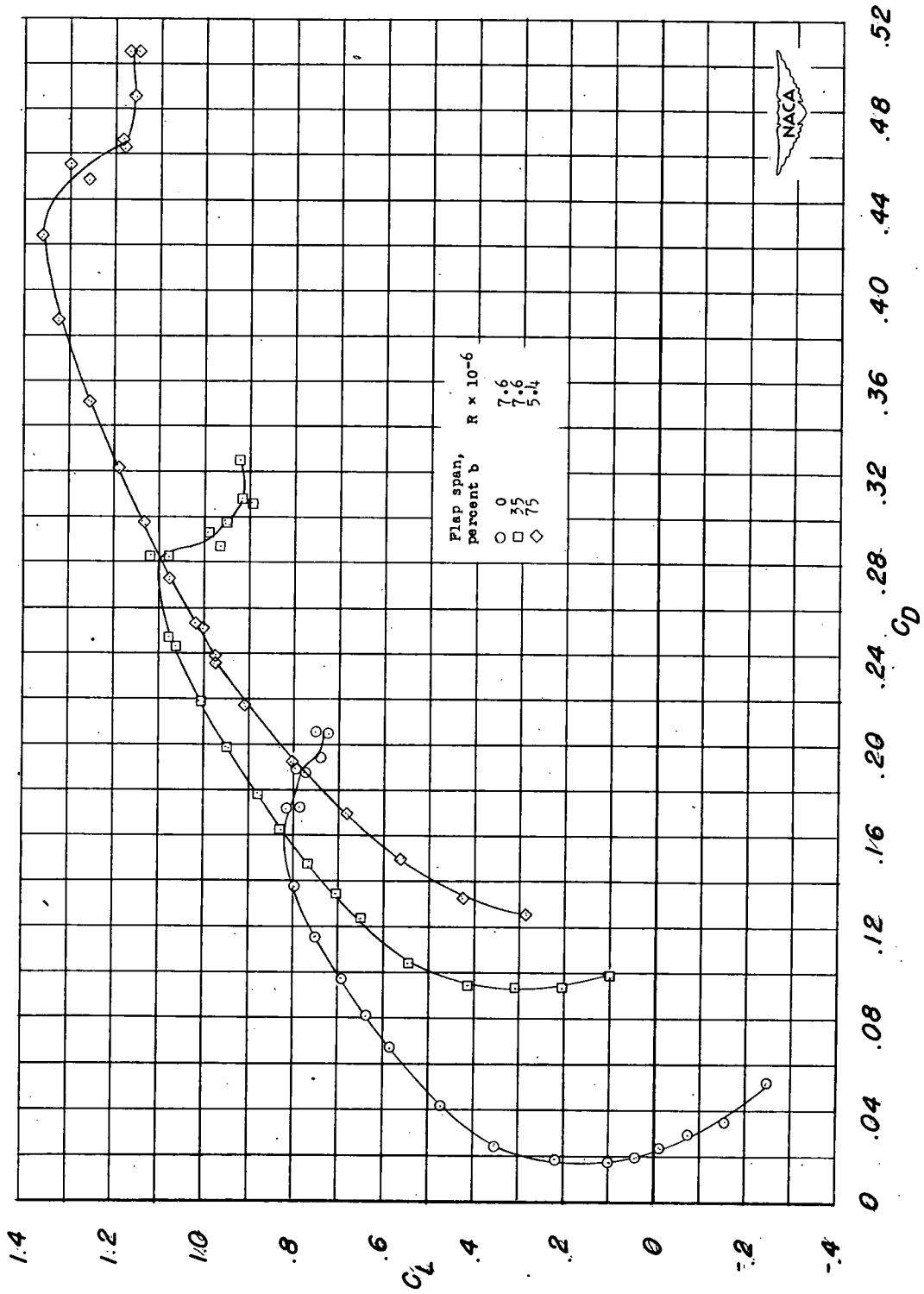


Figure 12.- Concluded.

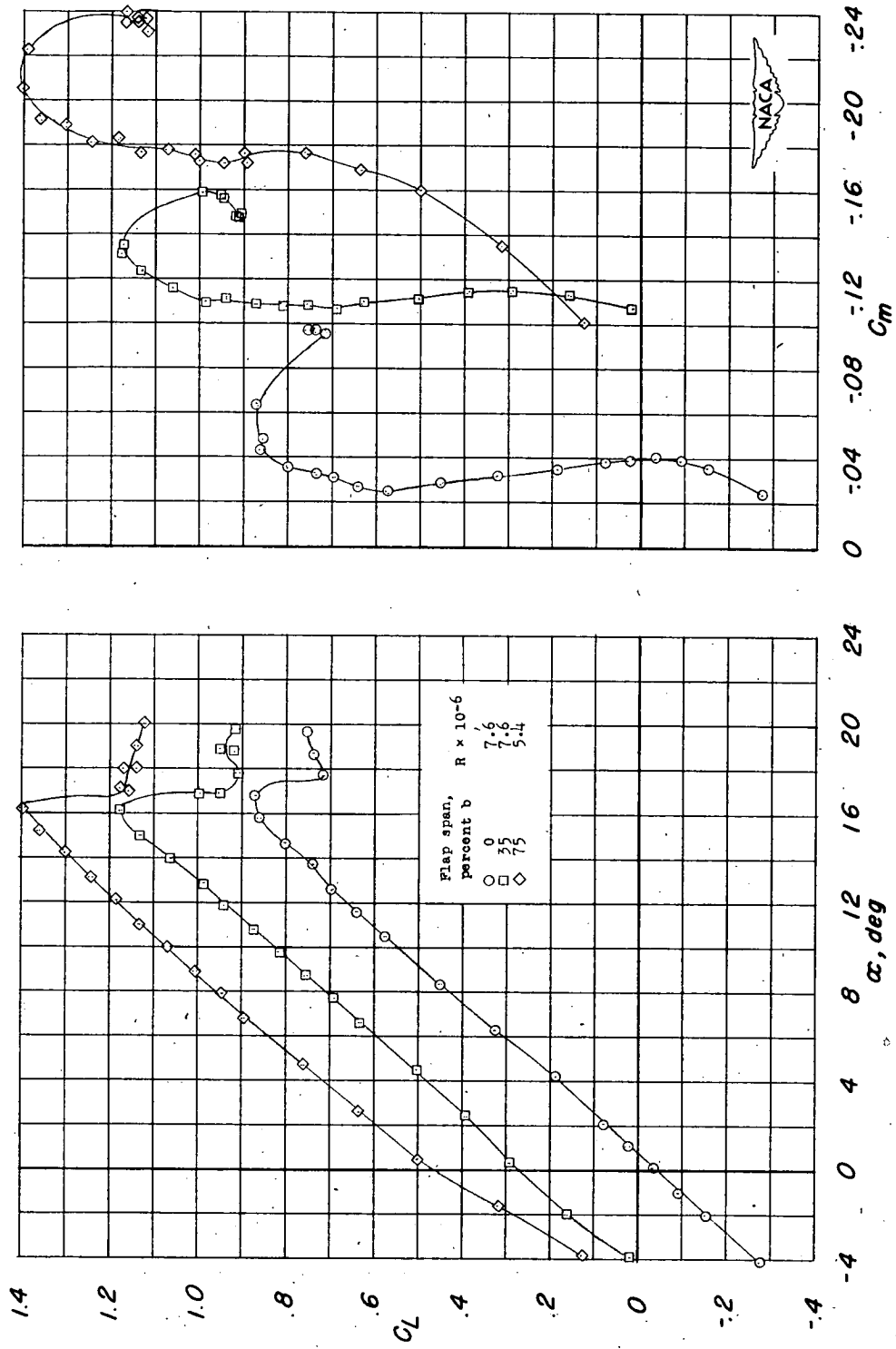


Figure 13.- Effect of plain flap span on the lift, drag, and pitching-moment characteristics of the wing with drooped-nose flaps deflected 30° . $\delta_f = 50^\circ$.

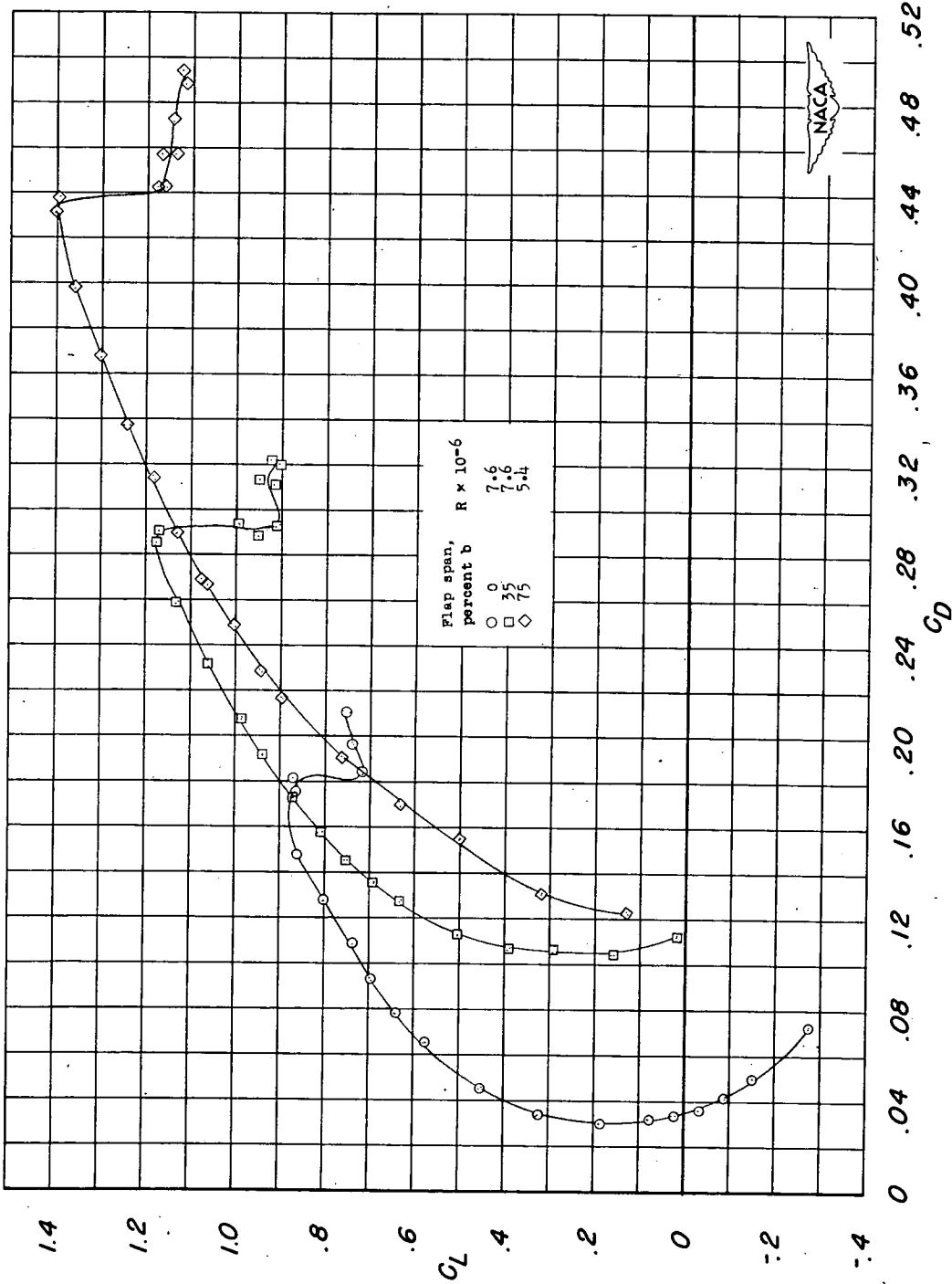
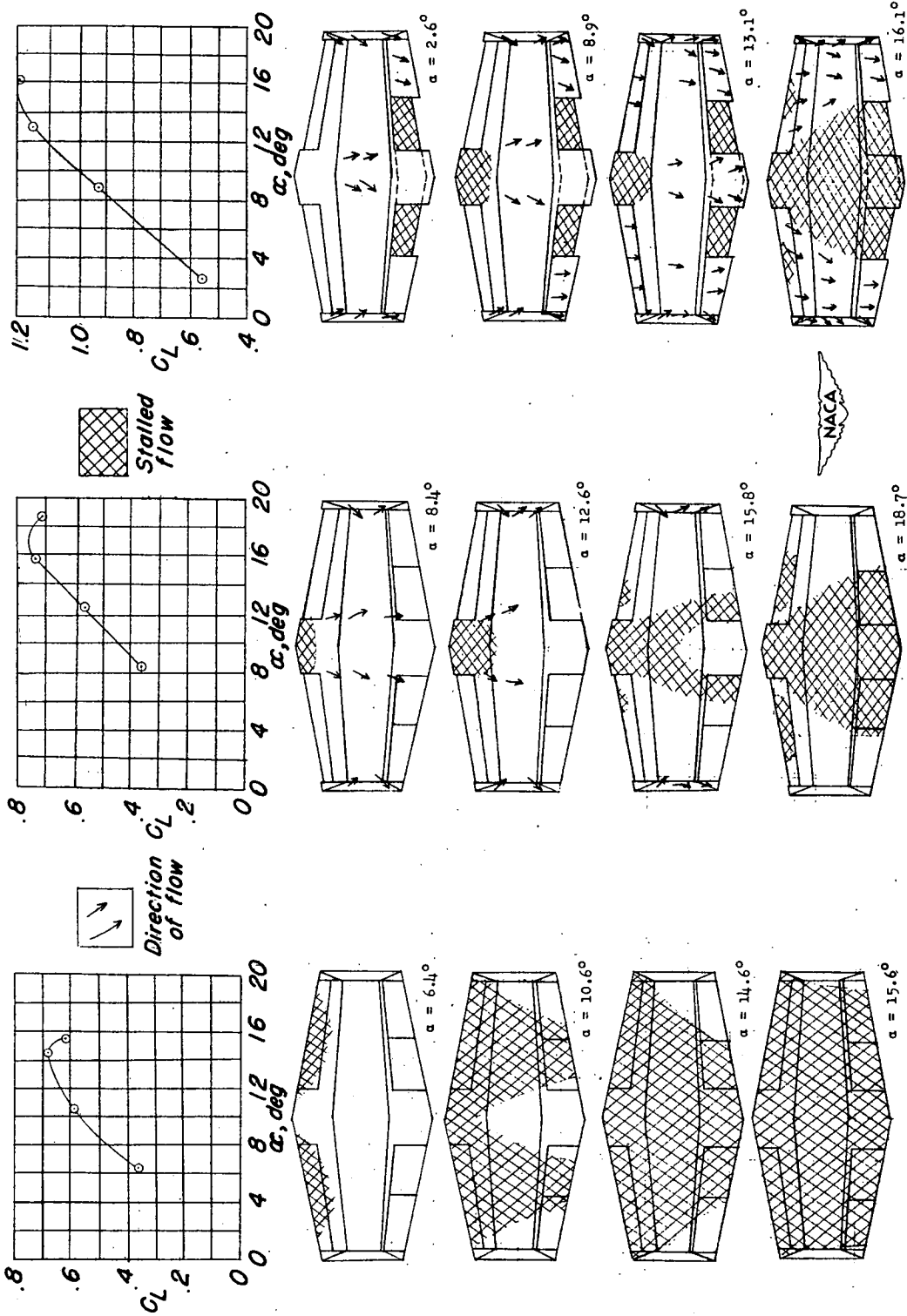


Figure 13.- Concluded.



(a) Plain wing.

(b) $\delta_n = 30^\circ$.

(c) $\delta_n = 30^\circ$; $\delta_f = 50^\circ$ (0.35b flaps).

Figure 14.- Stall patterns of hexagonal wing with and without flaps deflected.

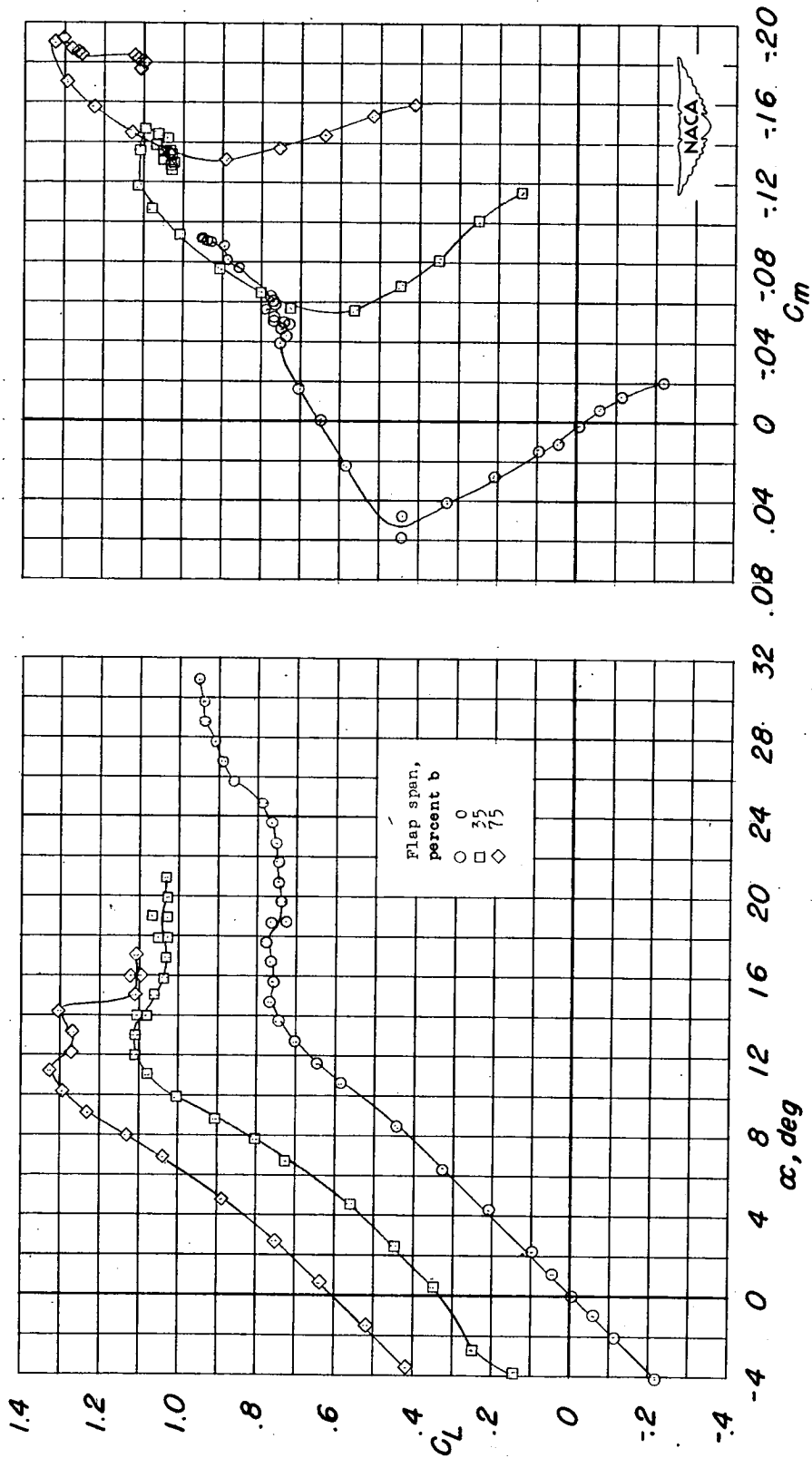


Figure 15.- Effect of plain flap span on the lift, drag, and pitching-moment characteristics of the wing-fuselage configuration. $\delta_f = 50^\circ$; $f_r = 8.0$; $R = 5.4 \times 10^6$.

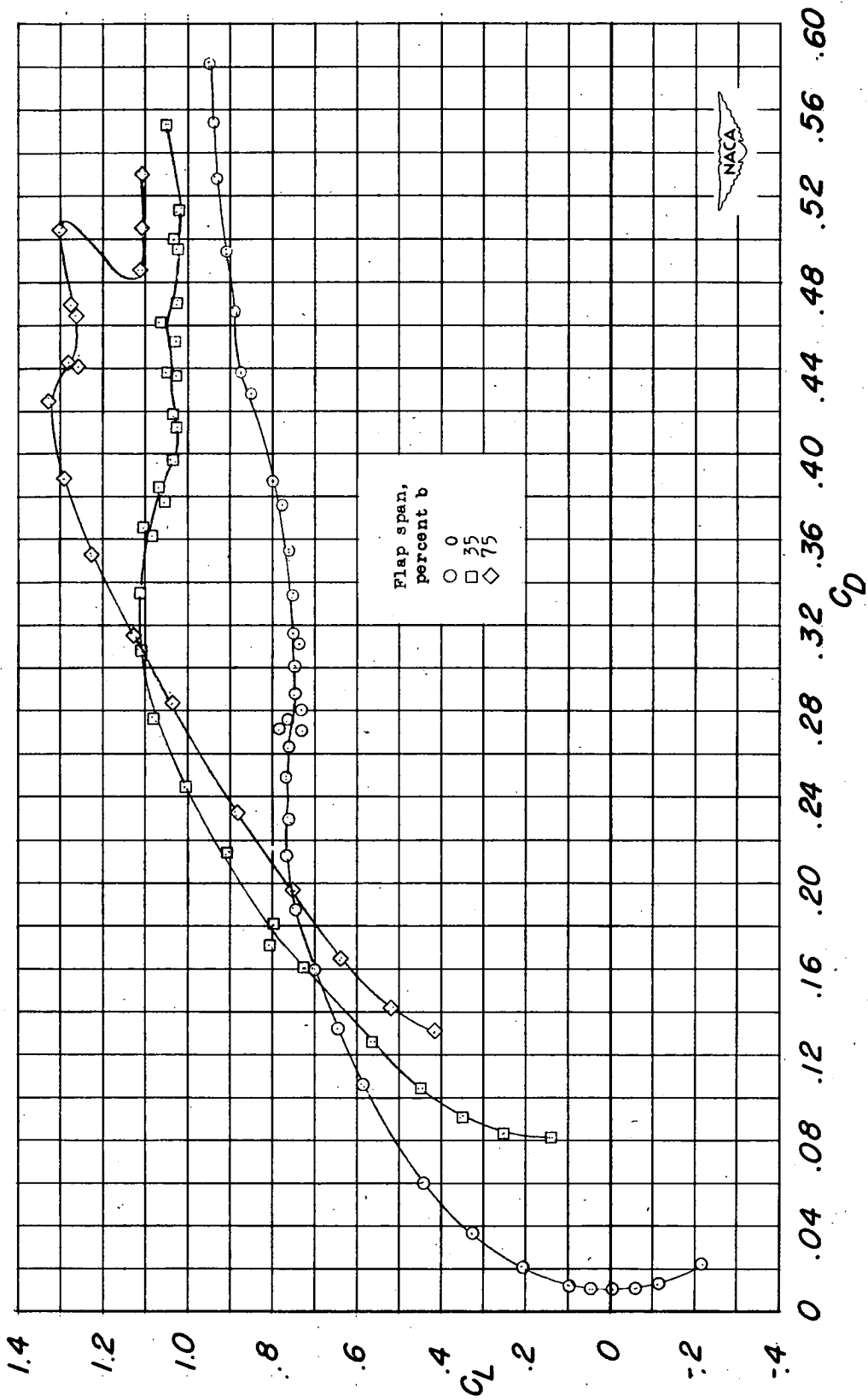


Figure 15.- Concluded.

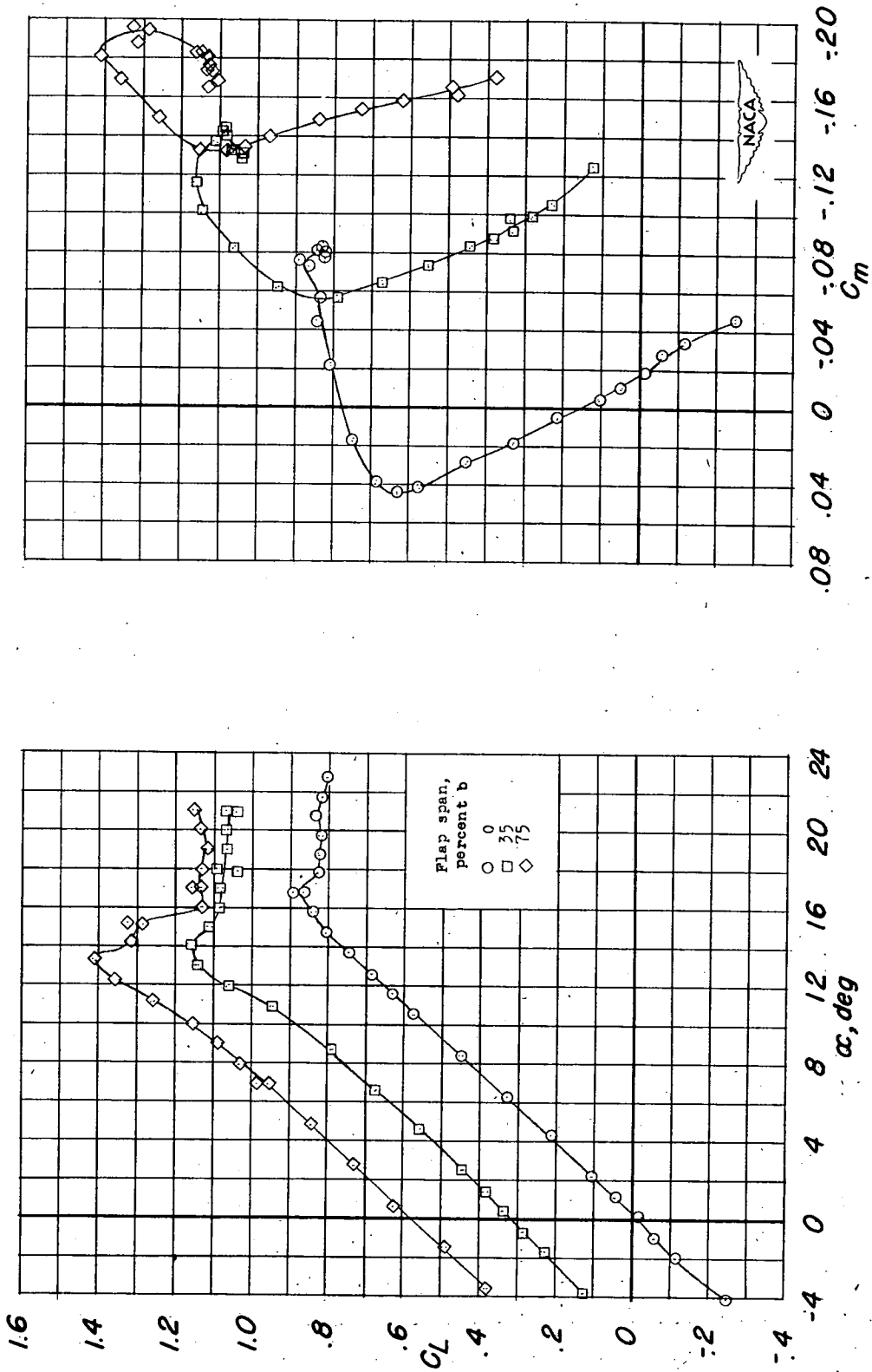


Figure 16.- Effect of plain flap span on the lift, drag, and pitching-moment characteristics of the wing-fuselage configuration with drooped-nose flaps deflected 10°. $\delta_f = 50^\circ$; $f_r = 8.0$; $R = 5.4 \times 10^6$.

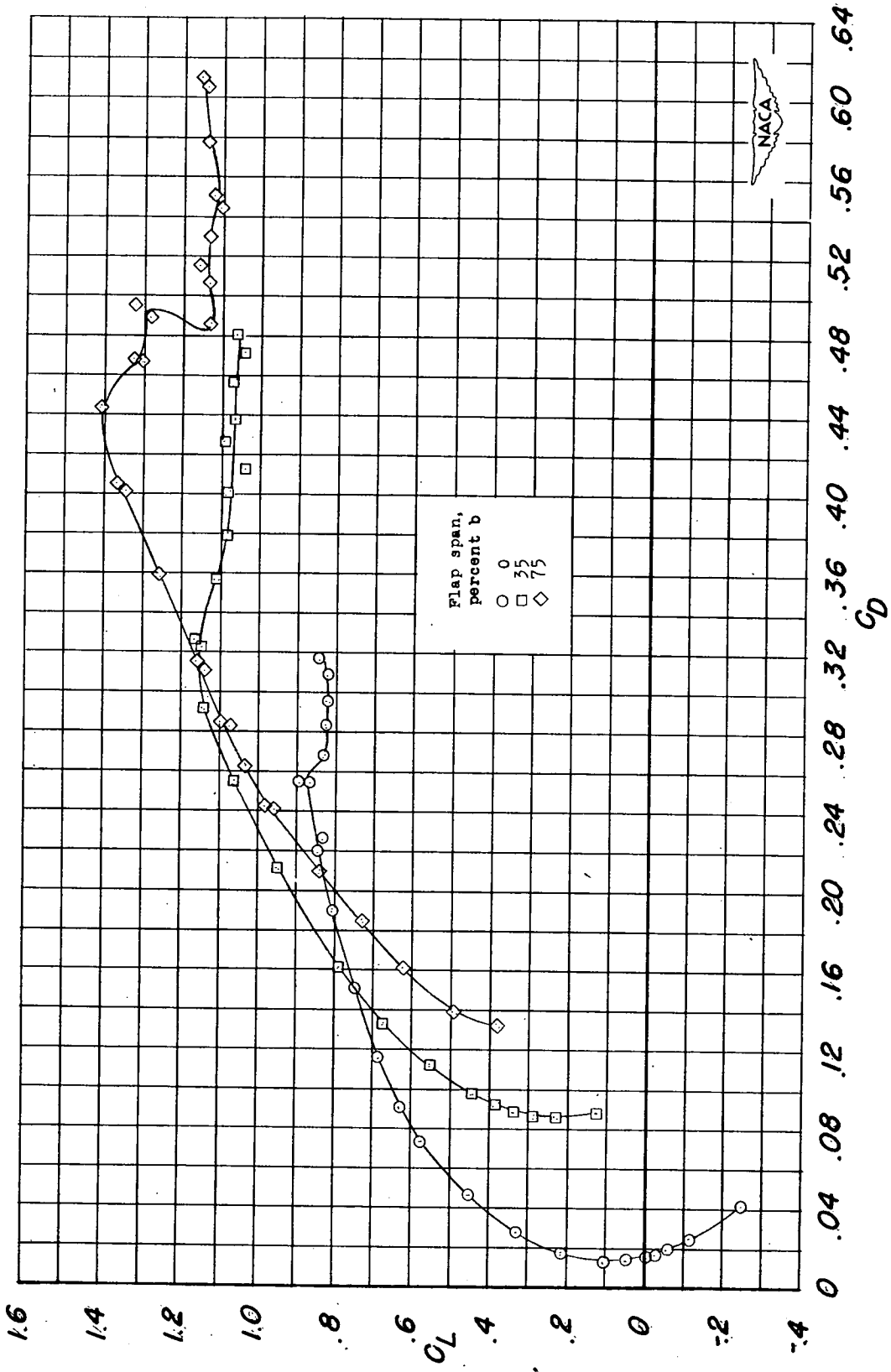


Figure 16.- Concluded.

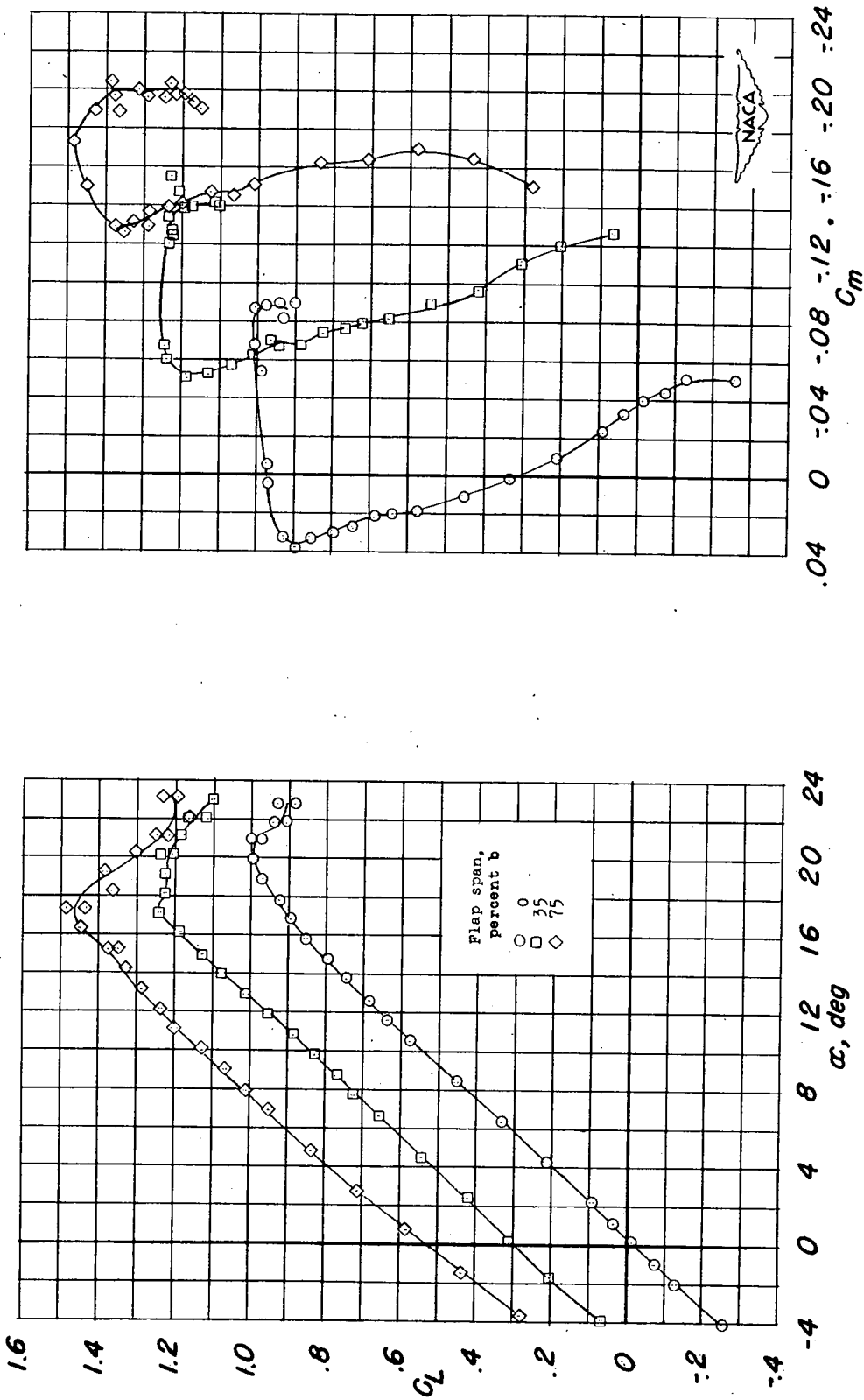


Figure 17.- Effect of plain flap span on the lift, drag, and pitching moment of the wing-fuselage configuration with drooped-nose flaps deflected 20°. $\delta_f = 50^\circ$; $f_r = 8.0$; $R = 5.4 \times 10^6$.

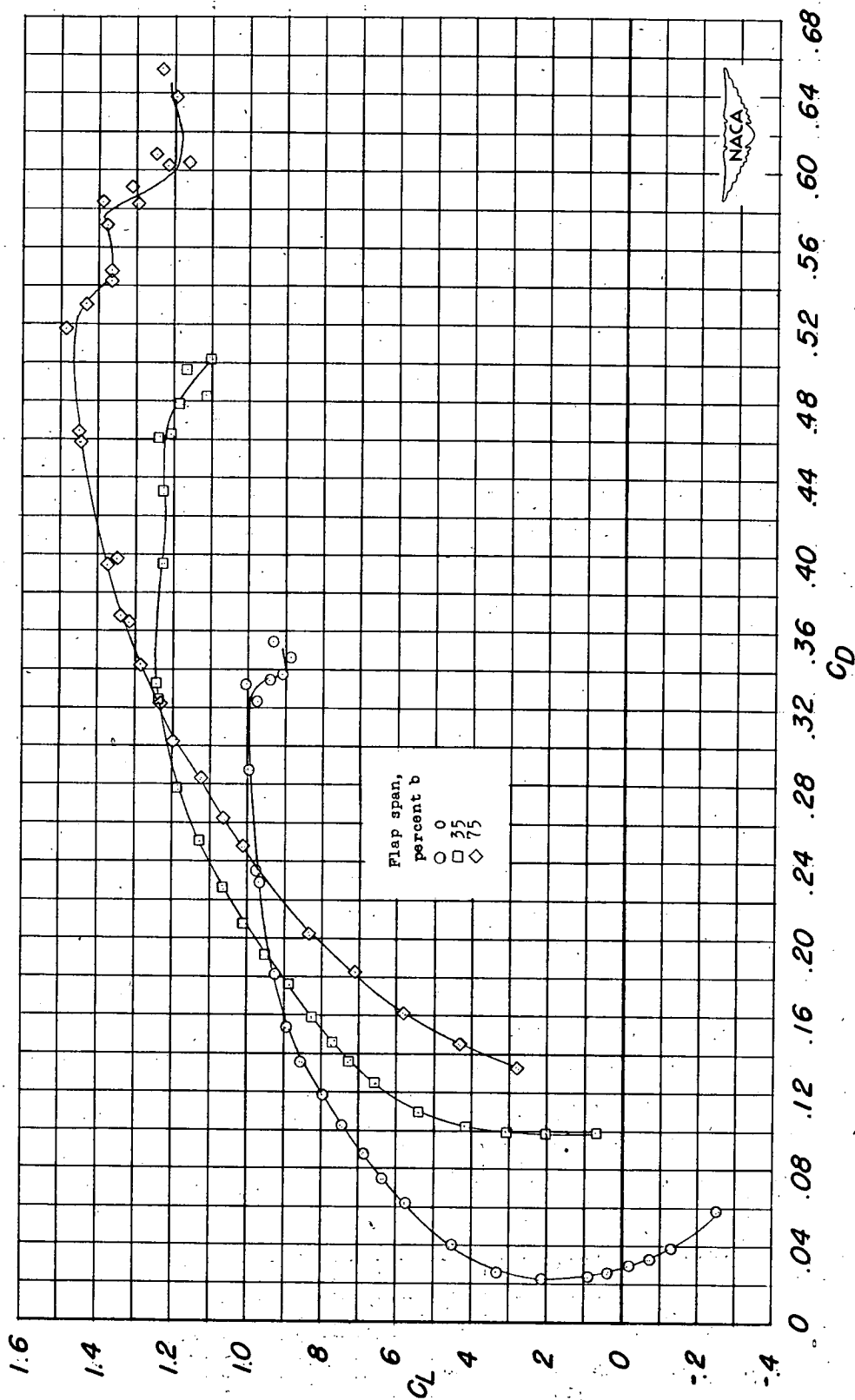


Figure 17.- Concluded.

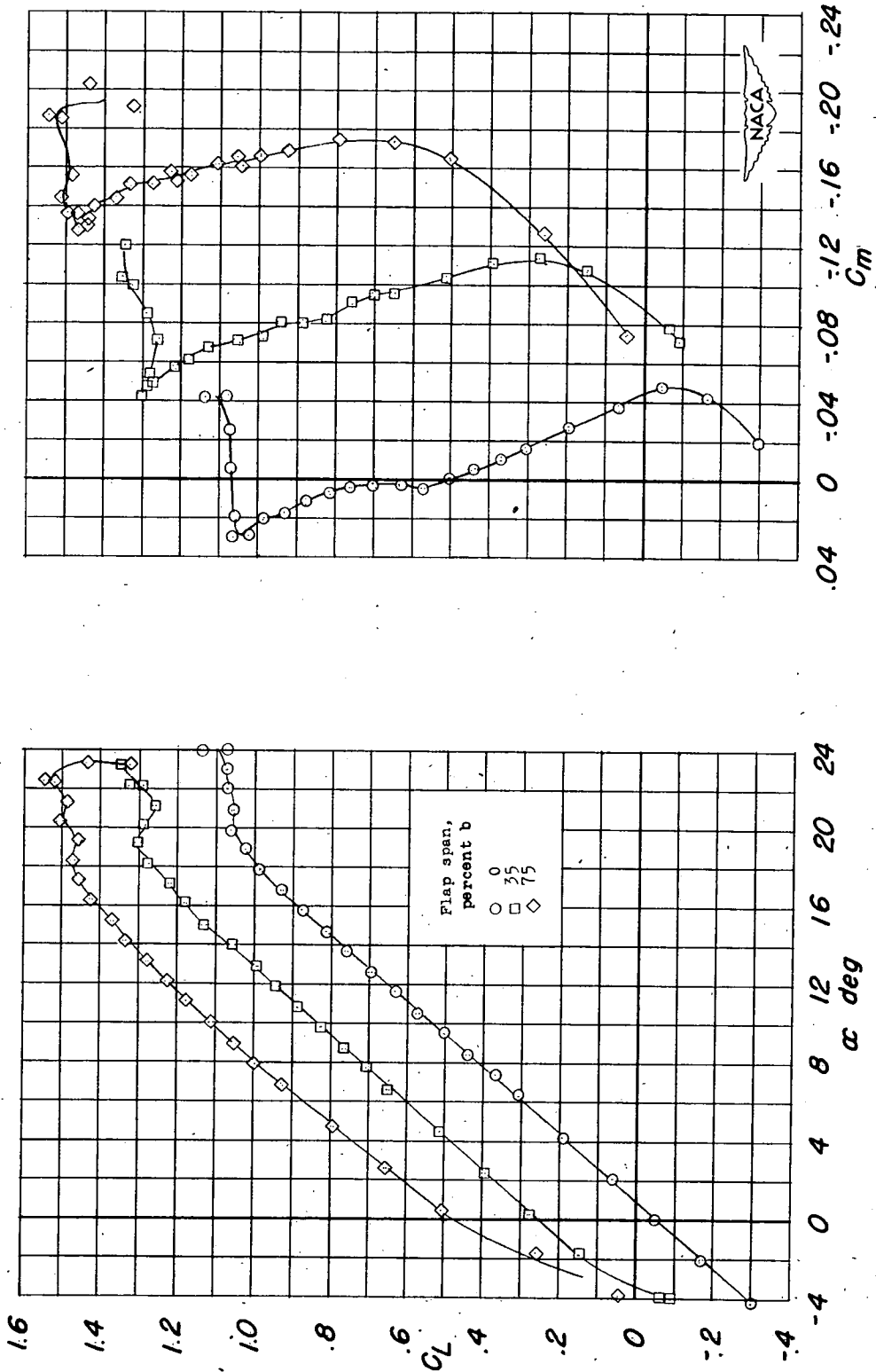


Figure 18.- Effect of plain flap span on the lift, drag, and pitching-moment characteristics of the wing-fuselage configuration with drooped-nose flaps deflected 30° . $\delta_f = 50^\circ$; $f_r = 8.0$; $R = 5.4 \times 10^6$.

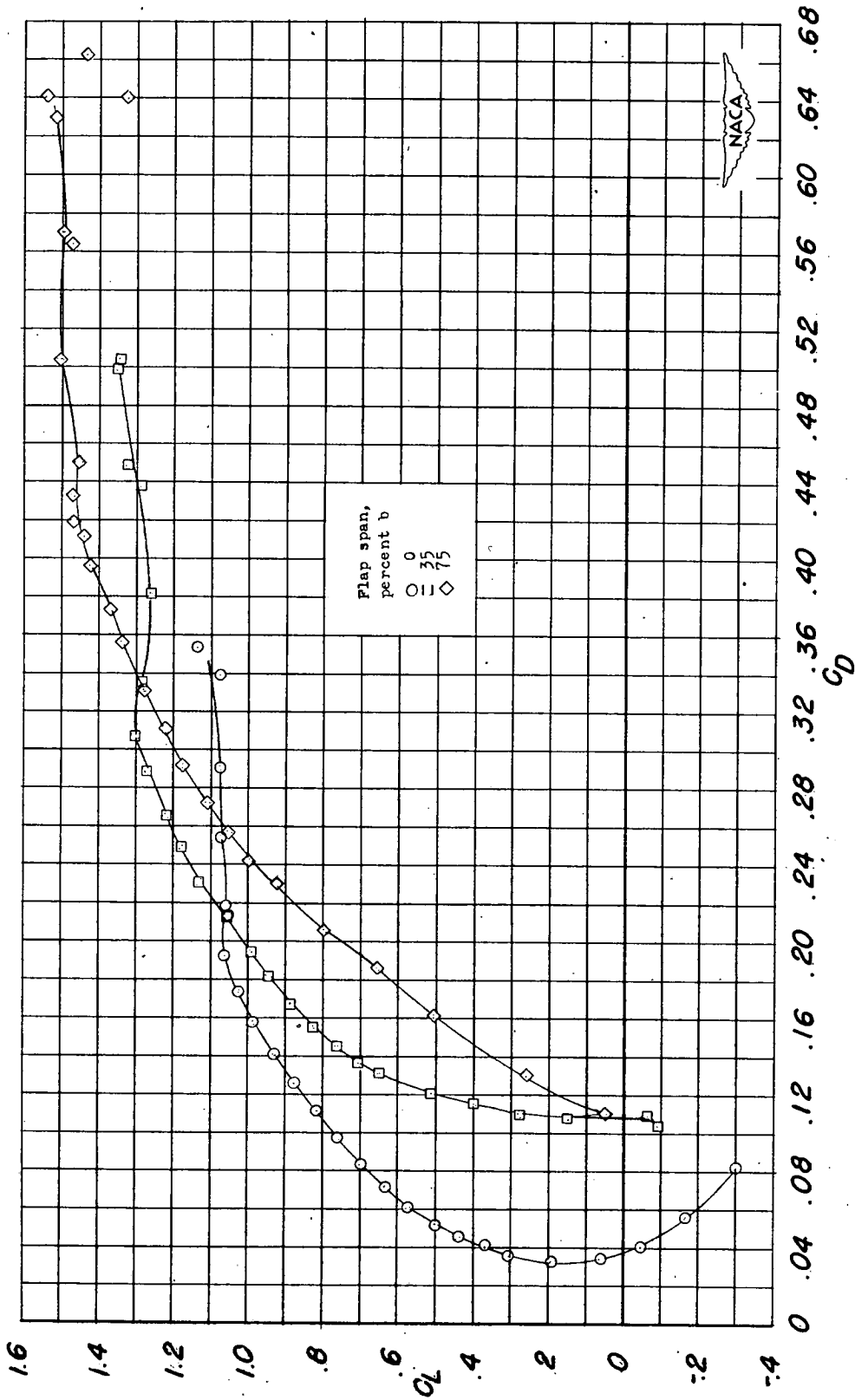
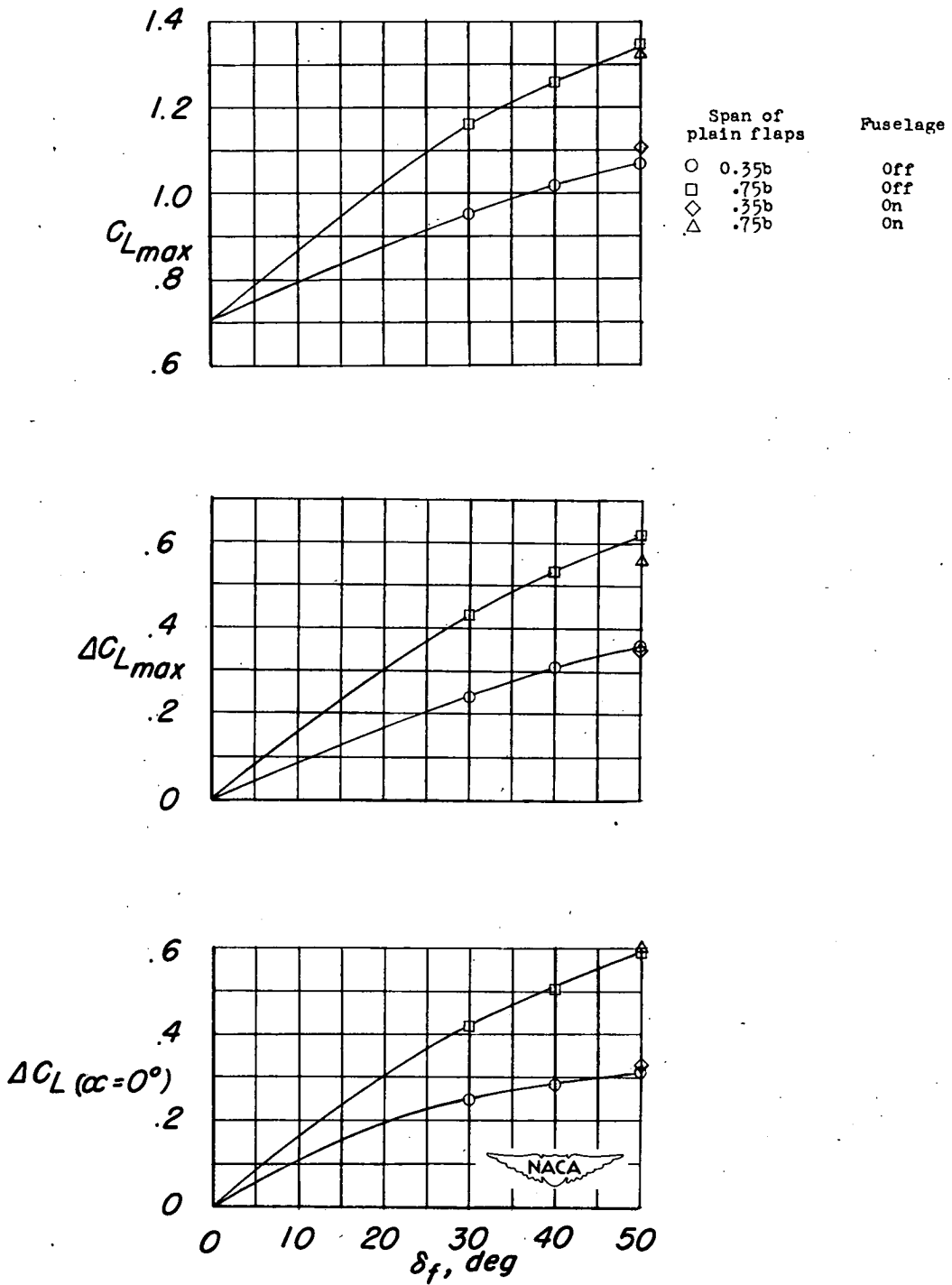
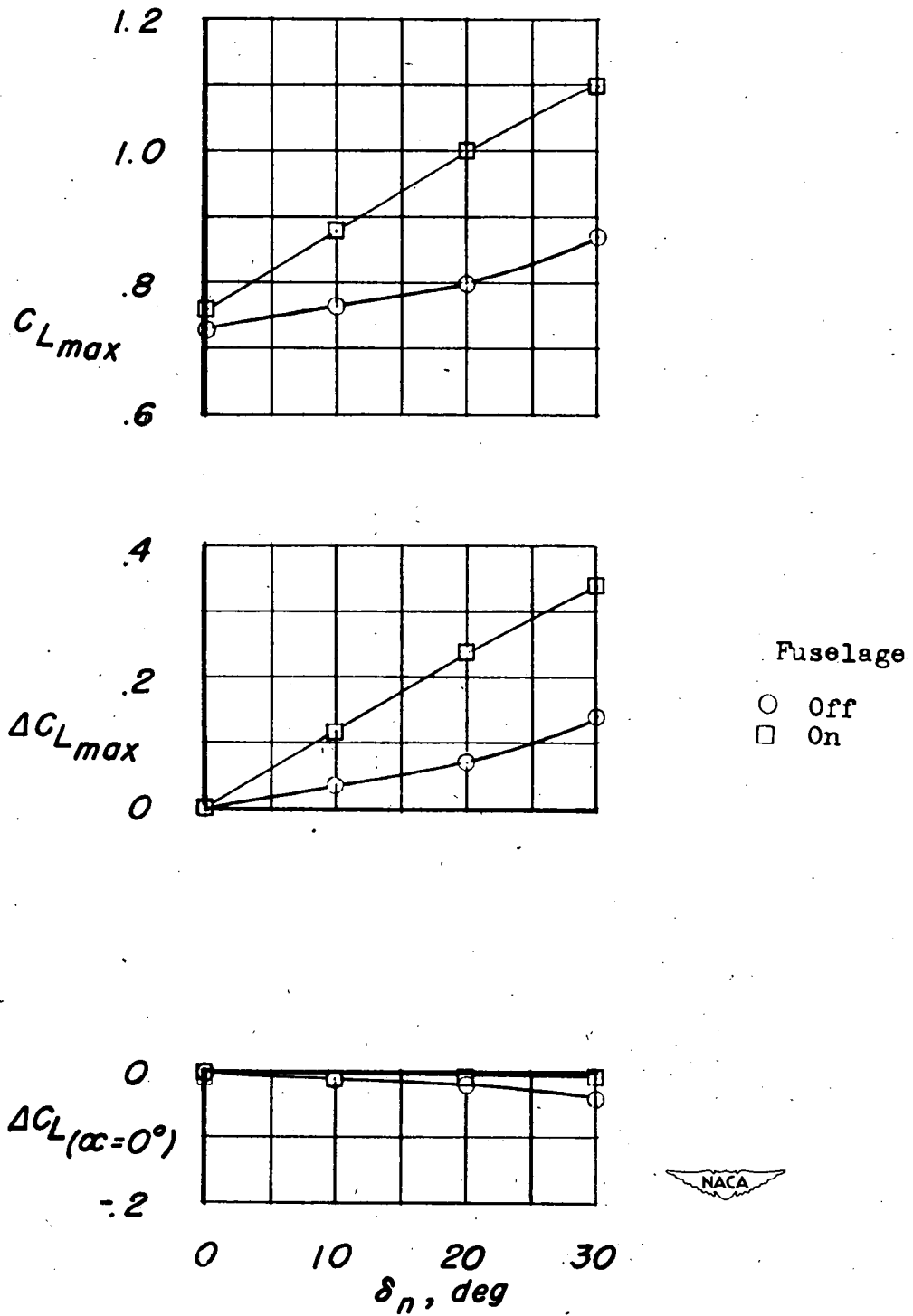


Figure 18.- Concluded.



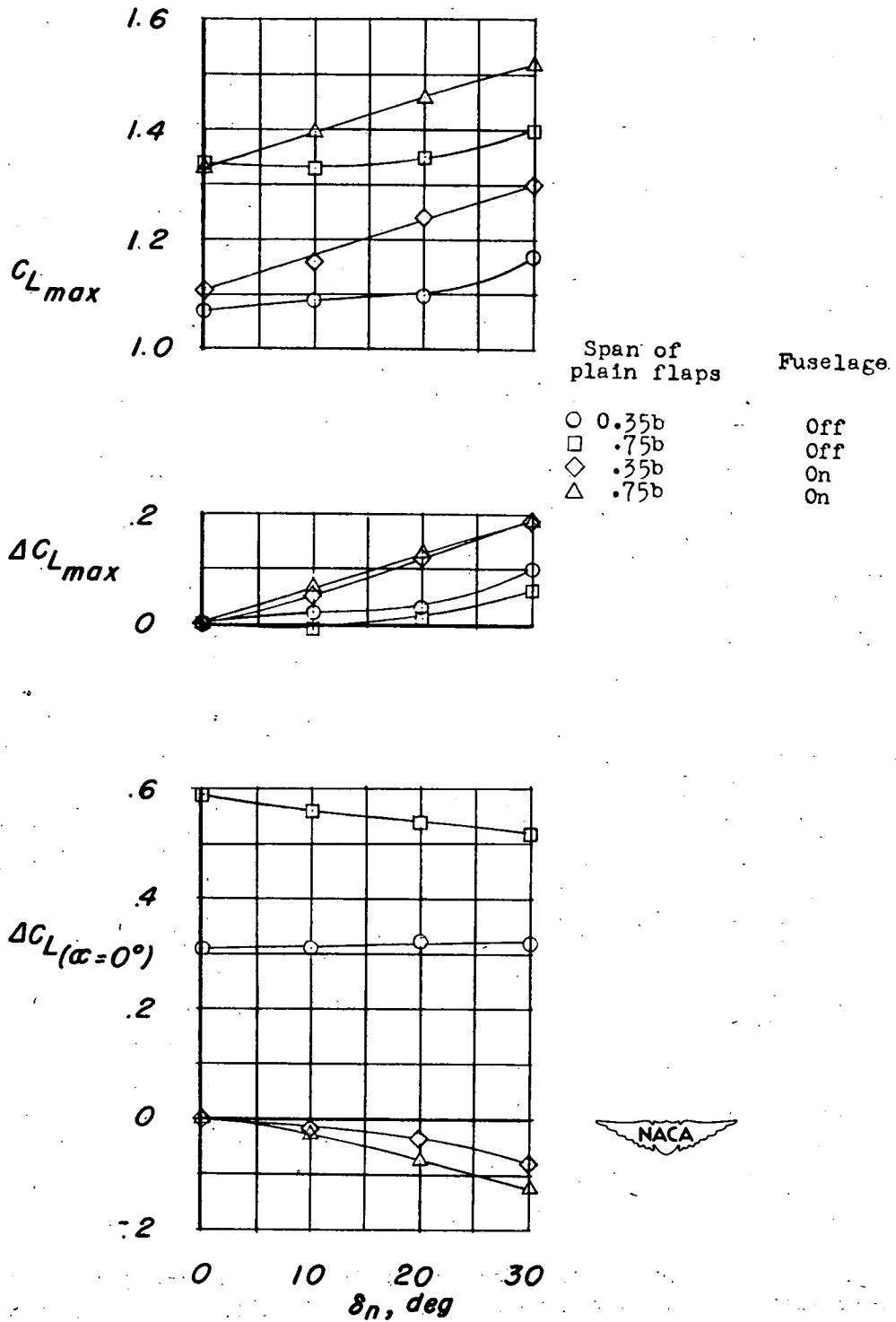
(a) Plain flaps deflected.

Figure 19.- Summary of the effects of flap deflection on the lift characteristics of the wing with and without fuselage.



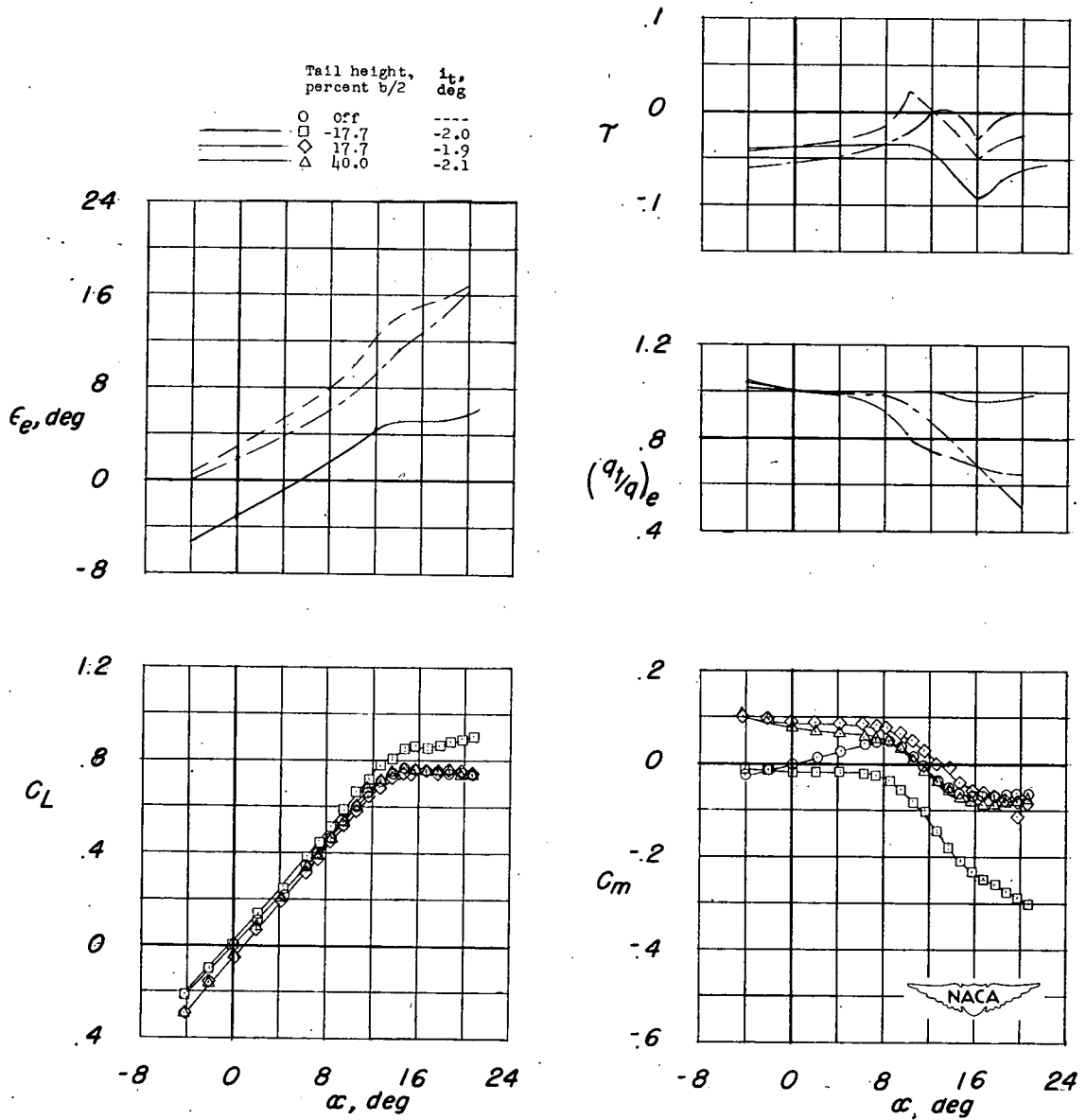
(b) Drooped-nose flaps.

Figure 19.- Continued.



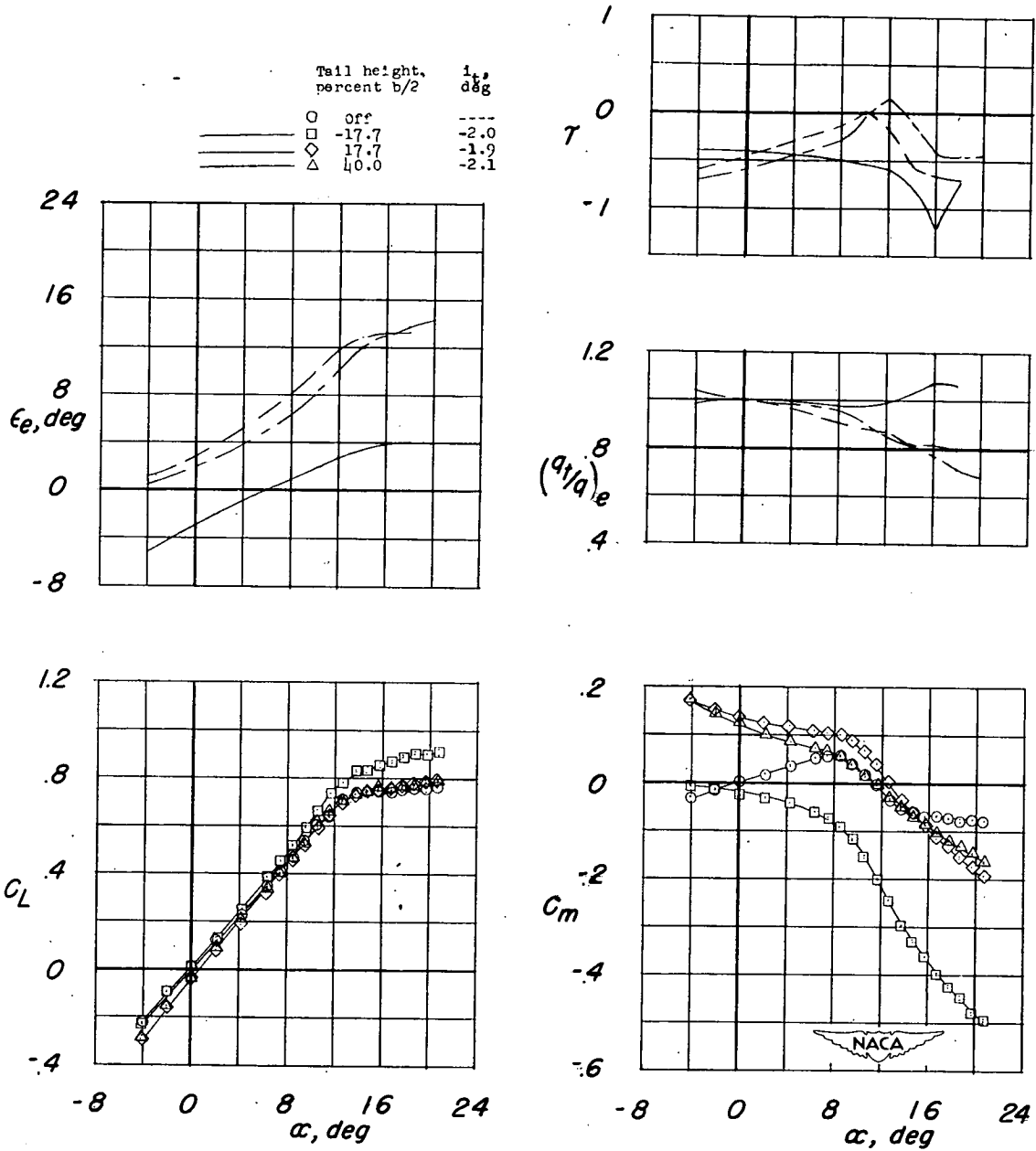
(c) Effect of drooped-nose flaps with plain flaps deflected 50°.

Figure 19.- Concluded.



(a) Tail length, $2\bar{c}$.

Figure 20.- Effect on the longitudinal stability characteristics of the plain wing-fuselage configuration of a horizontal tail located at various vertical positions. $R = 7.6 \times 10^6$.



(b) Tail length, $3\bar{c}$.

Figure 20.- Concluded.

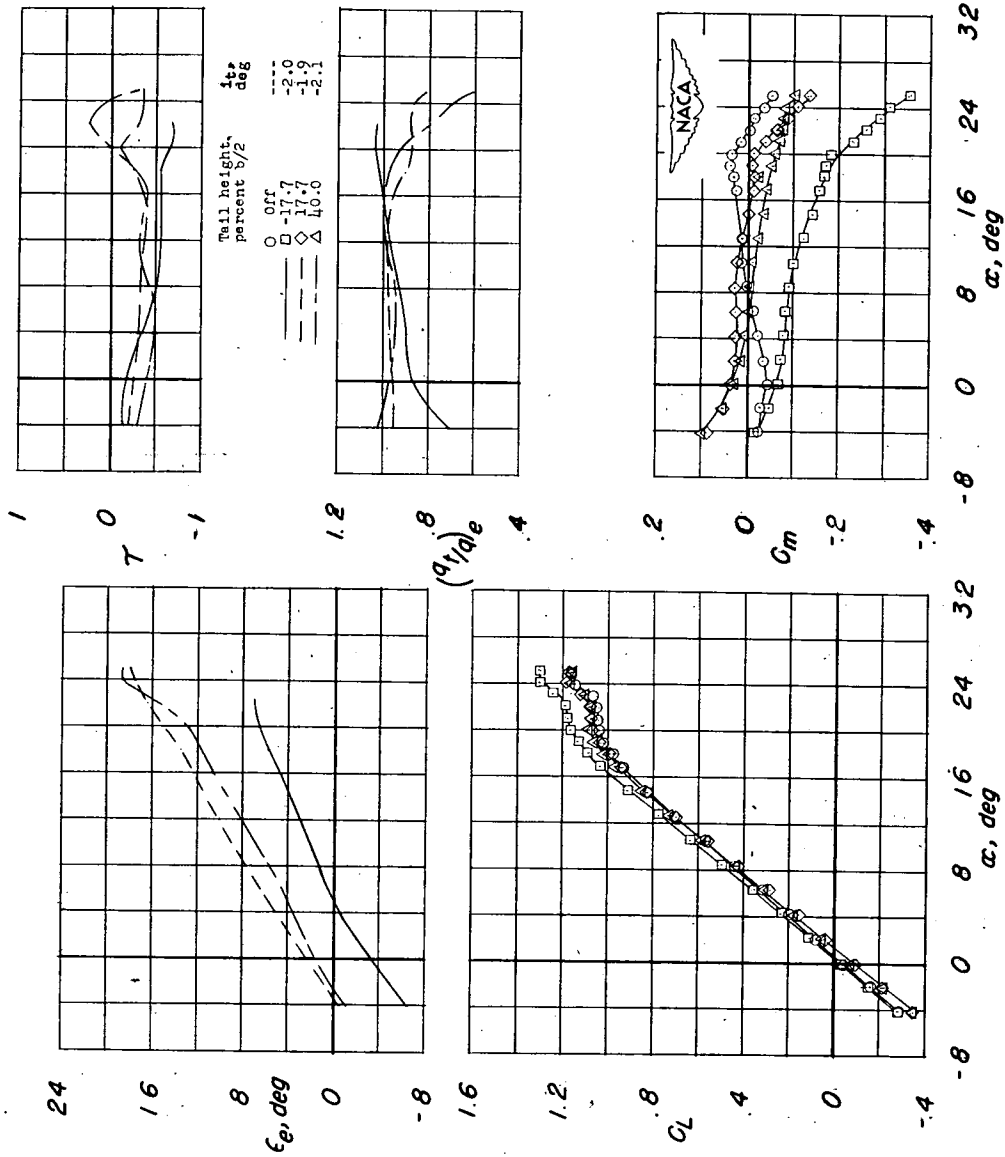
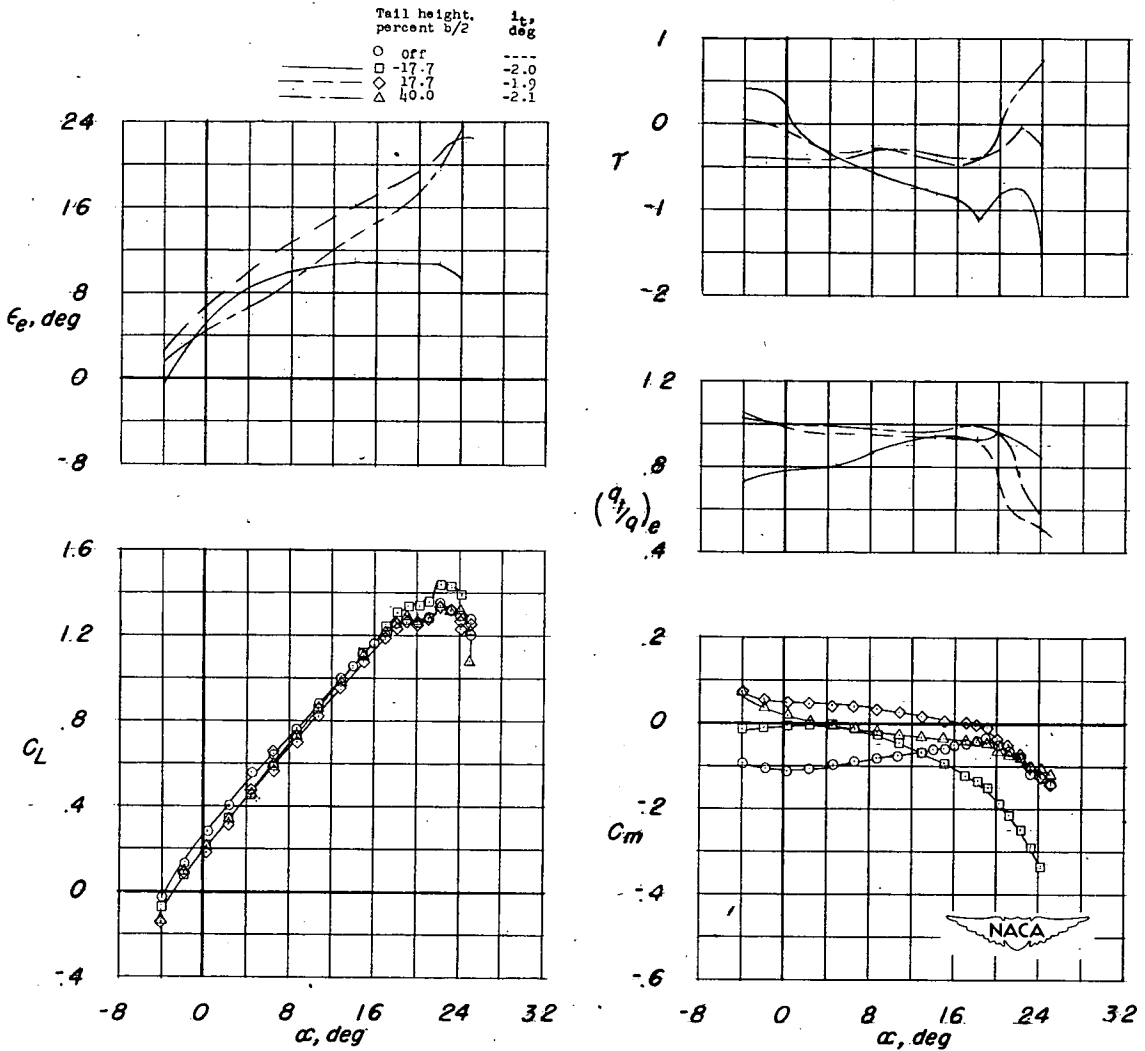


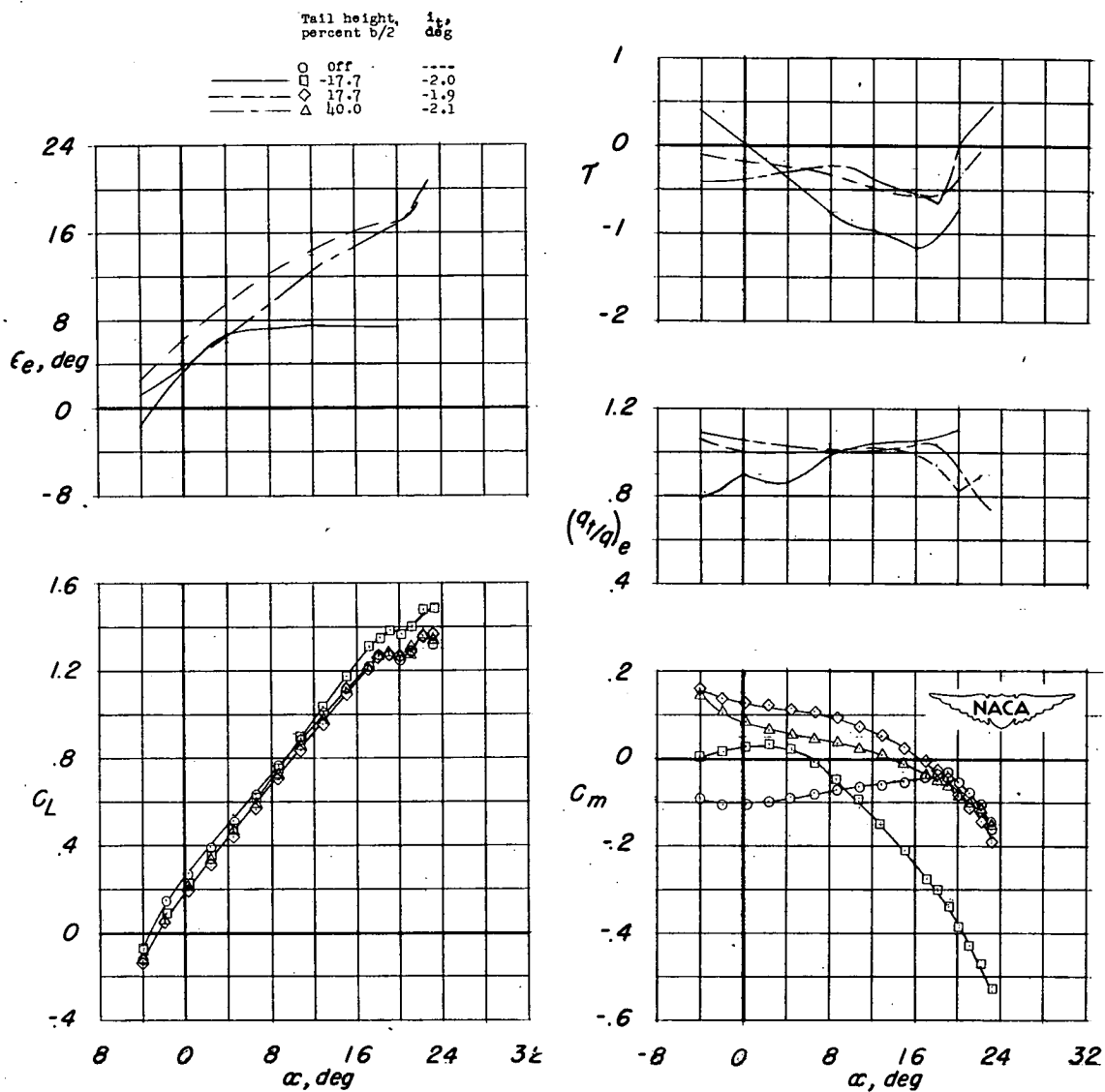
Figure 21.- Effect on the longitudinal characteristics of the wing-fuselage configuration with drooped-nose flaps deflected 30° of a horizontal tail located at various vertical positions. Tail length, $2\bar{c}$; $R = 7.6 \times 10^6$.



(a) Tail length, $2\bar{c}$.

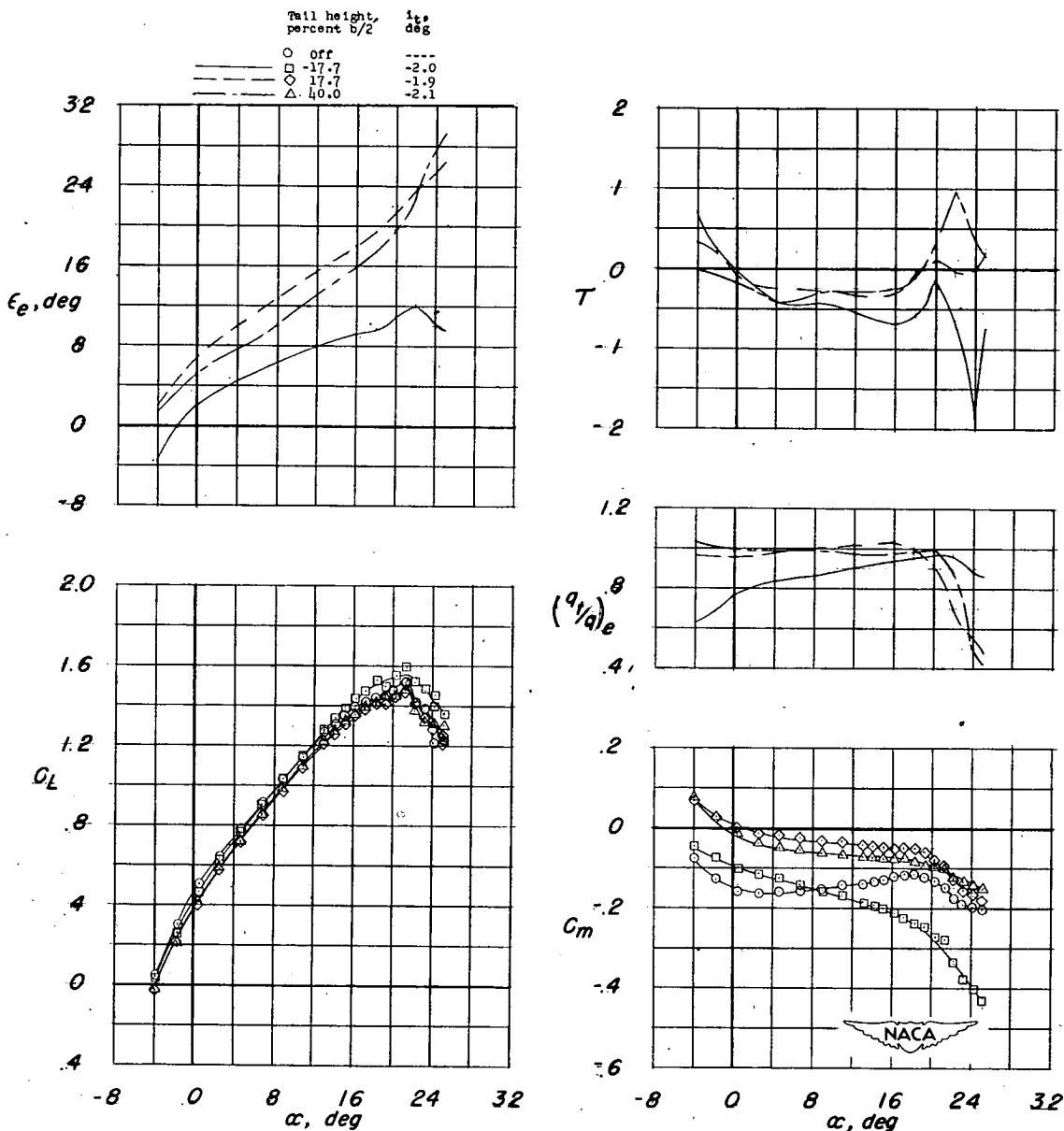
Figure 22.- Effect on the longitudinal stability characteristics of the wing-fuselage configuration with drooped-nose flaps and 0.35b plain flaps of a horizontal tail located at various vertical positions.

$\delta_n = 30^\circ$; $\delta_f = 50^\circ$; $R = 7.6 \times 10^6$.



(b) Tail length, $3\bar{c}$.

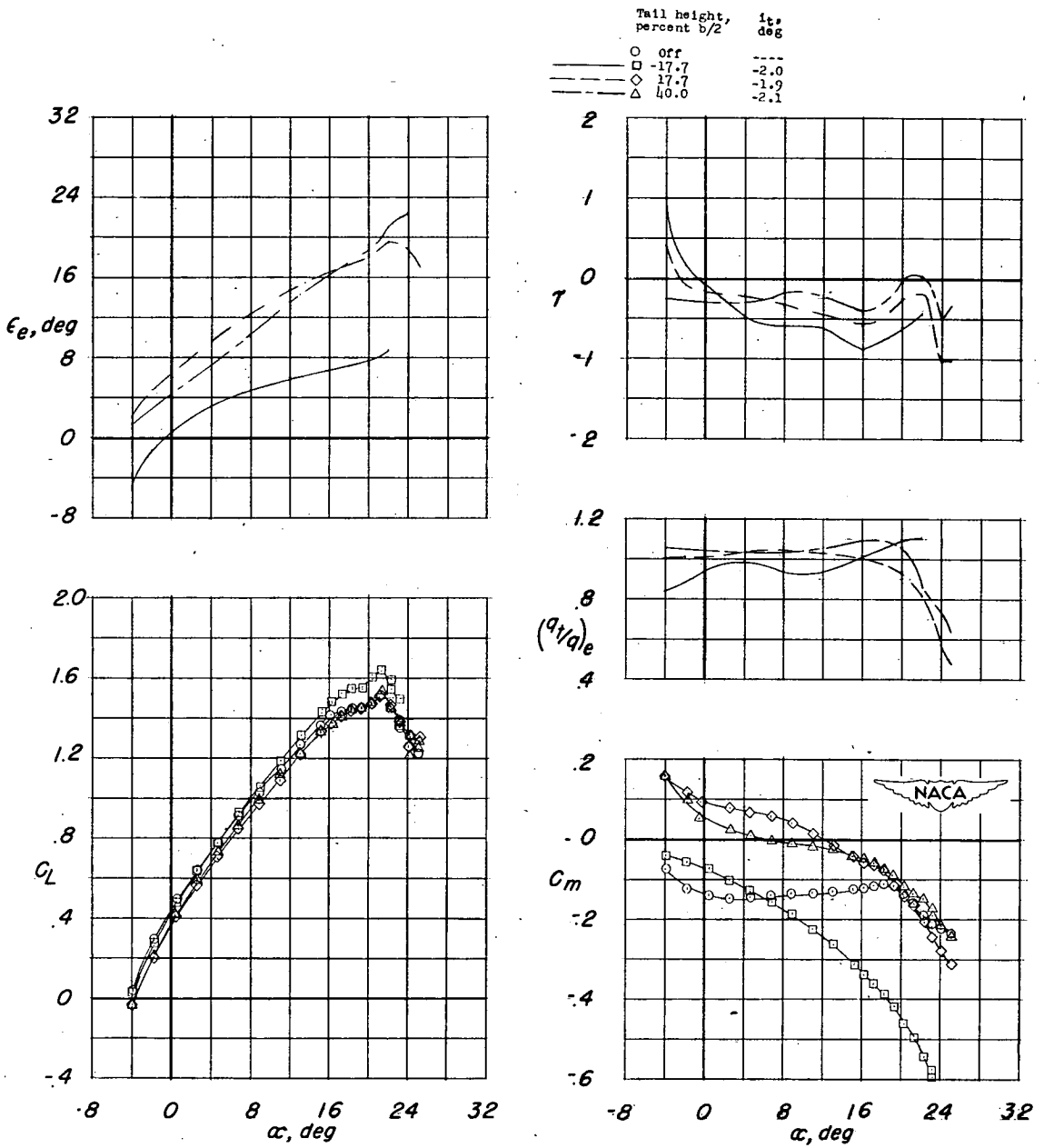
Figure 22.- Concluded.



(a) Tail length, $2\bar{c}$.

Figure 23.- Effect on the longitudinal stability characteristics of the wing-fuselage configuration with drooped-nose flaps and 0.75b plain flaps of a horizontal tail located at various vertical positions.

$\delta_n = 30^\circ$; $\delta_f = 50^\circ$; $R = 5.4 \times 10^6$.



(b) Tail length, $3\bar{c}$.

Figure 23.- Concluded.

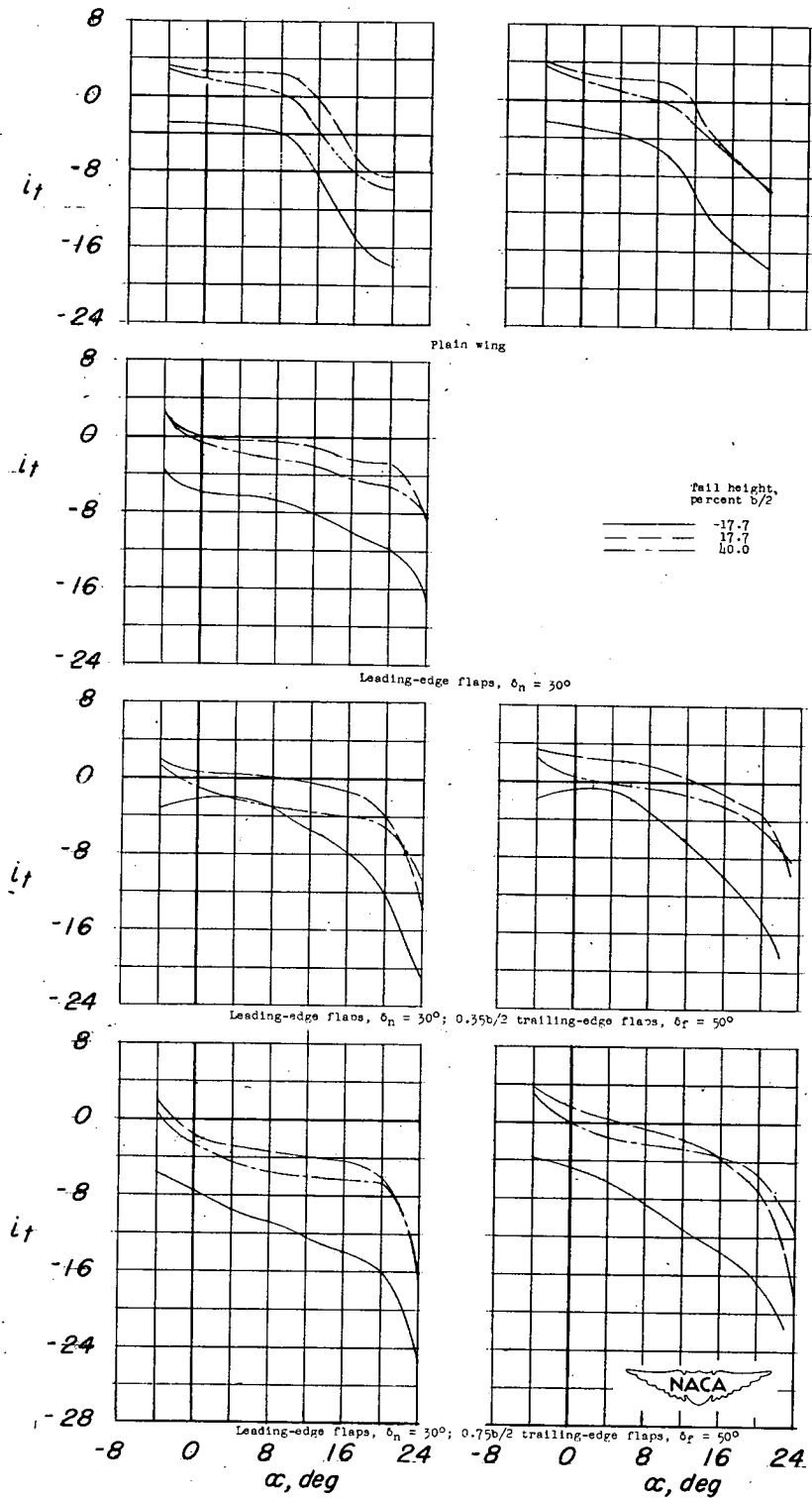


Figure 24.- Tail incidence required for trim; center of gravity located at $0.25\bar{c}$.